

Damage assessment of shear connectors with vibration measurements and power spectral density transmissibility

Jun Li^{*1}, Hong Hao^{1a}, Yong Xia^{2b} and Hong-ping Zhu^{3c}

¹Department of Civil Engineering, School of Civil and Mechanical Engineering, Curtin University, Bentley, WA 6102, Australia

²Department of Civil and Environmental Engineering, The Hong Kong Polytechnic University, Hung Hom, Kowloon, Hong Kong, People's Republic of China

³School of Civil Engineering and Mechanics, Huazhong University of Science and Technology, Wuhan, Hubei, People's Republic of China

(Received October 27, 2014, Revised March 9, 2015, Accepted March 12, 2015)

Abstract. Shear connectors are generally used to link the slab and girders together in slab-on-girder bridge structures. Damage of shear connectors in such structures will result in shear slippage between the slab and girders, which significantly reduces the load-carrying capacity of the bridge. Because shear connectors are buried inside the structure, routine visual inspection is not able to detect conditions of shear connectors. A few methods have been proposed in the literature to detect the condition of shear connectors based on vibration measurements. This paper proposes a different dynamic condition assessment approach to identify the damage of shear connectors in slab-on-girder bridge structures based on power spectral density transmissibility (PSDT). PSDT formulates the relationship between the auto-spectral densities of two responses in the frequency domain. It can be used to identify shear connector conditions with or without reference data of the undamaged structure (or the baseline). Measured impact force and acceleration responses from hammer tests are analyzed to obtain the frequency response functions at sensor locations by experimental modal analysis. PSDT from the slab response to the girder response is derived with the obtained frequency response functions. PSDT vectors in the undamaged and damaged states can be compared to identify the damage of shear connectors. When the baseline is not available, as in most practical cases, PSDT vectors from the measured response at a reference sensor to those of the slab and girder in the damaged state can be used to detect the damage of shear connectors. Numerical and experimental studies on a concrete slab supported by two steel girders are conducted to investigate the accuracy and efficiency of the proposed approach. Identification results demonstrate that damages of shear connectors are identified accurately and efficiently with and without the baseline. The proposed method is also used to evaluate the conditions of shear connectors in a real composite bridge with in-field testing data.

Keywords: condition assessment; shear connectors; power spectral density transmissibility; structural monitoring; slab-on-girder bridge; frequency response function

*Corresponding author, Lecturer, E-mail: junli@curtin.edu.au

^aProfessor, E-mail: hong.hao@curtin.edu.au

^bAssociate Professor, E-mail: cexxia@polyu.edu.hk

^cProfessor, E-mail: hpzhu@mail.hust.edu.cn

1. Introduction

Structures may deteriorate with time and will continuously accumulate damage during their services due to aging, material deterioration, natural hazard such as earthquakes, storms, fires, long-term fatigues under heavy loads and corrosions. The unnoticed and uncorrected anomalies could potentially produce further damage and finally lead to catastrophic structural failures with a huge loss of properties. Therefore the interest to monitor a structure for detecting local damage at an early stage is prevailing throughout the civil engineering community. Measured vibration data are usually used for the condition assessment of civil structures. Generally, vibration-based damage detection methods could be classified into non-model based (direct correlation) and model-based (model updating). Non-model based methods compares the measured structural dynamic characteristics from the undamaged and damaged structures for identification, while model-based methods require the finite element model of the structure for iterative updating to make the analytical and measured structural vibration properties as close as possible. One major difficulty of model-based methods is that an accurate finite element model of undamaged structure is required for the identification, which is usually not available in practice. Many sources of uncertainties that would be introduced into the structure during their construction and service stages make it not easy to obtain a finite element model of the structure that closely represents the true structural conditions as the basis of model updating analysis for structural damage identification.

A structure can be considered as a dynamic system with stiffness, mass and damping components. Once some damages occur in the structure, the structural physical properties (i.e., stiffness, mass and damping) will change, and modal parameters of the structure will also change. Therefore, the changes in the structural vibration characteristics, such as natural frequencies (Salawu 1997), mode shapes (Gorl and Link 2003), mode shape curvature (Pandey *et al.* 1991), flexibility matrix (Yan *et al.* 2010), modal strain energy (Yan *et al.* 2012), frequency response function (FRF) (Maia *et al.* 2003), power spectral density function (Liberatore and Carman 2004, Xu and Wu 2007), and energy based damage index (Yi *et al.* 2014, Yi *et al.* 2013) etc., can be used to indicate the existence of damage and to identify the location and severity of damage.

Many bridges are built as the slab-on-girder structures. The concrete slab is supported on the concrete or steel girders, and stirrups are embedded in the girders and cast into the slab as shear connectors to link the slab and girders together. The shear connection between slab and girders in composite structures subjects to the major consequences of stress, overloading and fatigue, especially for large structures such as bridges. It follows that damages usually involve a deterioration or break of the shear connection in some regions of the structure, causing a decrease of the overall rigidity of the composite structure and a reduction of its ultimate resistance (Dilena and Morassi 2004). Damage of shear connectors in slab-on-girder structures will result in shear slippage between the slab and girder, which significantly reduces the load-carrying capacity of the bridge. Condition assessment of shear connectors is of great interest and important to evaluate the structural integrity in health monitoring of slab-on-girder structures. Xia *et al.* (2007) proposed a local detection method by directly comparing the frequency response functions of simultaneously measured vibrations on the slab and girder. It has been found that the local method would give better identification results than global methods, since the global modal information may not be sensitive to the local damage of shear connectors. The proposed local detection approach is extended to assess the integrity condition of shear connectors in real slab-on-girder bridges with in-field testing data (Xia *et al.* 2008). Recently, wavelet based Kullback-Leibler distance (Zhu *et*

al. 2014) and wavelet packet energy (Ren *et al.* 2008) have also been proposed for damage identification of shear connectors. Liu and De Roeck (2008) proposed a local condition assessment approach to identify the damage location of shear connectors by using the modal curvature and wavelet transform modulus maxima. Berczynski and Wroblewski (2010) validated the numerical models of steel-concrete composite beams with experimental testing results and later energy transfer ratio was used to locate the damage in composite beams (Wroblewski *et al.* 2013). Dilena and Morassi (2009) investigated the damage detection problems with partially degraded shear connection in steel-concrete composite beams.

The generalized transmissibility matrix for a multi-degrees-of-freedom system in frequency domain has been proposed by Ribeiro *et al.* (2000). Studies on dynamic response reconstruction in a substructure using the generalized transmissibility concept in frequency domain and its use for damage identification have been presented (Li *et al.* 2012). The relationship between two sets of response vectors in frequency domain is formulated. A structural health monitoring methodology based on novelty detection with measured transmissibility from the structure was proposed (Worden and Manson 2003). The use of transmissibility functions for damage detection has also been explored (Johnson and Adams 2002) by using system zeros in the transfer function as indicators to detect the damage. Later, the transmissibility concept is developed in the wavelet domain (Li and Law 2011). This wavelet-based transmissibility defines the relationship between two time domain response vectors, and is used for the substructure damage identification (Li and Law 2012). Yan and Ren (2011) proposed the power spectrum density transmissibility to identify the modal parameters. Transmissibility between cross-spectral densities of two output responses with respect to a reference response is formulated to extract the natural frequencies and mode shapes of the structure under operational conditions.

In this paper, the power spectral density transmissibility (PSDT) is further developed between the auto-spectral densities of two responses in the frequency domain, and used to detect conditions of shear connectors. Measured impact force and acceleration responses from hammer tests are analyzed to obtain the FRFs at the slab and girder sensor locations by experimental modal analysis. Then PSDT from the slab response to the girder response is derived with the obtained FRFs. If the measurement data from the undamaged structure are available, PSDT vectors in the undamaged and damaged states are compared to identify the damage of shear connectors. When the measurement data from the undamaged structure are not available, a reference sensor is defined and PSDT vectors from the reference sensor response to the slab and girder responses respectively in the damaged state are used to identify the damage of shear connectors. Numerical and experimental studies on a concrete slab supported by two steel girders are conducted to investigate the performance of the proposed approach. The proposed method is also used to evaluate the conditions of shear connectors in a real composite bridge with in-field testing data.

2. Damage detection with existing methods

In order to demonstrate the superiority of the proposed method, commonly used vibration-based methods are also used to identify shear connector conditions. These methods are briefly reviewed here.

2.1 Coordinate modal assurance criteria

Coordinate Modal Assurance Criteria (COMAC) describes the correlation of mode shapes with respect to an individual point over all the modes. For point q , the COMAC is defined as (Lieven and Ewin 1988)

$$\text{COMAC}(\phi^u, \phi^d, q) = \frac{\left(\sum_{i=1}^{nm} |(\phi_i^u)_q (\phi_i^d)_q| \right)^2}{\left(\sum_{i=1}^{nm} (\phi_i^u)_q^2 \right) \left(\sum_{i=1}^{nm} (\phi_i^d)_q^2 \right)} \quad (1)$$

where ϕ^u and ϕ^d are the structural mode shapes in the undamaged and damaged states; $(\phi_i^u)_q$ and $(\phi_i^d)_q$ represent the i th mode shape values at point q from the undamaged and damaged structures and nm is the number of mode shapes involved in the COMAC computation. Normally a low COMAC value indicates a worse correlation between two mode shapes and a possible existence of the damage around the point.

2.2 Modal flexibility

The modal flexibility matrix can be estimated from the measured modal frequencies and normalized mode shapes (Pandey and Biswas 1994) as

$$F = \sum_i^{nm} \frac{1}{\omega_i^2} \{\phi_i\} \{\phi_i\}^T \quad (2)$$

where F is the flexibility matrix, ω_i is the i th modal frequency, ϕ_i is the i th mode shape and nm is the number of mode shapes.

If two sets of measurements, one from the intact structure and another from the damaged structure, are taken and modal parameters are identified from the measurements, the flexibility matrix for the two cases can be obtained and change in the flexibility matrix Δ can be calculated as

$$\Delta = F_i - F_d \quad (3)$$

where F_i and F_d are the flexibility matrices for the intact and damaged cases, respectively. For each measurement location j , let $\bar{\delta}_j$ be the maximum absolute value of the elements in the corresponding column Δ , i.e.

$$\bar{\delta}_j = \max_i |\delta_{ij}| \quad (4)$$

where δ_{ij} are elements of the j th column of Δ . To detect and locate damage in a structure, the quantity $\bar{\delta}_j$ is used as the measure of change of flexibility for each measurement location.

2.3 Relative difference of frequency response functions between slab and girder

The abovementioned two methods are global detection methods by comparing the identified modal information from intact and damaged structures. They need the baseline information. A

local method has been proposed (Xia *et al.* 2008) based on the relative difference of the frequency response functions (RDFRF) between the slab and girder from the existing structure only, which is used to evaluate the condition of the shear connectors. RDFRF is defined as

$$\text{RDFRF}(H_i^G, H_i^S) = \frac{\left\| \{H_i^G\} - |\{H_i^S\}| \right\|}{\left\| \{H_i^G\} + |\{H_i^S\}| \right\|} \quad (5)$$

where H_i is the frequency response function at the i th point; superscript G and S denote that sensor points are on the girder and slab, respectively; $\|\cdot\|$ is the Euclidean norm and $|\cdot|$ is the absolute value (or magnitude of the complex numbers). The calculation of frequency response function will be given in Section 3.1. A high RDFRF value means a significant difference in the responses at a particular point, which indicates the damage in the vicinity.

3. Damage detection with power spectral density transmissibility

The formulation of PSDT will be derived and its use for damage identification of shear connectors in slab-on-girder structures will be developed. Two cases are considered in this paper. The first assumes that the measured responses from the reference state (undamaged structure) are available. The other assumes that no measurement data from the reference structure is available, which is more practical in real applications to condition assessment of existing structures because measured responses from the structures in the undamaged state are normally not available.

3.1 Frequency response function

The general equation of motion of a damped structure with n degrees-of-freedom (DOFs) can be written as

$$M\{\ddot{x}(t)\} + C\{\dot{x}(t)\} + K\{x(t)\} = \{F(t)\} \quad (6)$$

where M , C and K are the $n \times n$ mass, damping and stiffness matrices of the structure, respectively; $\{\ddot{x}(t)\}$, $\{\dot{x}(t)\}$ and $\{x(t)\}$ are respectively the nodal acceleration, velocity and displacement vectors of the structure; $\{F(t)\}$ is a vector of applied forces at the associated DOFs of the structure. Rayleigh damping $C = a_1M + a_2K$ is assumed in this study, where a_1 and a_2 are the Rayleigh damping coefficients.

The Fourier transform of Eq. (6) gives

$$(-\omega^2 M + j\omega C + K)X(\omega) = F(\omega) \quad (7)$$

Therefore, the displacement response in frequency domain is given as

$$X(\omega) = H_a(\omega)F(\omega) = (-\omega^2 M + j\omega C + K)^{-1} F(\omega) \quad (8)$$

in which, $H_a(\omega) = (-\omega^2 M + j\omega C + K)^{-1}$ is the displacement FRF matrix. FRF represents the inherent system frequency response characteristics and it can be measured experimentally, reconstructed from an experimental modal analysis, or obtained from a finite element analysis of the structure.

The acceleration response in frequency domain could be obtained from Eq. (7) as

$$\ddot{X}(\omega) = -\omega^2 X(\omega) = H_a(\omega)F(\omega) = -\omega^2 H_d(\omega)F(\omega) \quad (9)$$

where $H_a(\omega) = -\omega^2 H_d(\omega)$ is the acceleration FRF matrix. In this study, the acceleration FRF is obtained from the measured input force and output acceleration responses. The modal frequencies, mode shapes, and damping ratios are extracted from the FRFs with the DIAMOND toolbox (Doebeling *et al.* 1997) in Matlab environment using the rational fraction polynomial method (Ewins 2000).

3.2 Power spectral density transmissibility in a structure

The PSDT between the cross-spectral densities of two output responses with respect to a reference response is formulated, and has been used for operational modal analysis (Yan and Ren 2011). In this study, PSDT is modified by defining it between the auto-spectral densities of two output responses in the frequency domain, and no reference output response is required in the formulation.

Assuming that $G_{FF}(\omega)$ is the auto-spectral density function of the input excitation force on the structure, $G_{\ddot{x}_i \ddot{x}_i}(\omega)$ and $G_{\ddot{x}_j \ddot{x}_j}(\omega)$ are the auto-spectral density functions of output acceleration responses at sensor locations i and j , respectively. The following equation can be obtained (Bendat and Piersol 1980)

$$\begin{cases} G_{\ddot{x}_i \ddot{x}_i}(\omega) = |H_a^i(\omega)|^2 G_{FF}(\omega) \\ G_{\ddot{x}_j \ddot{x}_j}(\omega) = |H_a^j(\omega)|^2 G_{FF}(\omega) \end{cases} \quad (10)$$

where, $H_a^i(\omega)$, $H_a^j(\omega)$ are the FRFs at the sensor location i and j , respectively, and they are complex vectors. The response reconstruction equation between two power spectral density functions can be obtained as

$$G_{\ddot{x}_j \ddot{x}_j}(\omega) = PSDT(\omega) G_{\ddot{x}_i \ddot{x}_i}(\omega) \quad (11)$$

in which, $PSDT(\omega)$ is the power spectral density transmissibility from the auto-spectral density $G_{\ddot{x}_i \ddot{x}_i}(\omega)$ at the sensor location i to the auto-spectral density $G_{\ddot{x}_j \ddot{x}_j}(\omega)$ at location j . $PSDT(\omega)$ can be expressed as

$$PSDT(\omega) = \frac{|H_a^j(\omega)|^2}{|H_a^i(\omega)|^2} \quad (12)$$

Eq. (12) formulates the concept of PSDT between the auto-spectral density functions of two responses in frequency domain and it can be obtained from the FRFs of the structure. Therefore, PSDT is a function of system parameters and an inherent characteristic. It may be noted that PSDT is a vector with scalar numbers at all the frequency lines ω in the spectrum.

3.3 Case 1: damage detection with measured data from undamaged structure available

A local condition assessment approach is proposed based on the fact that when damage occurs in shear connectors, the slab separates from the beam and the response on the slab may not be exactly the same as that on the girder. Therefore the differences in responses can be used to detect the shear connector damage. When the measurement data from the undamaged structure are available, PSDT vectors from the slab response to the girder response in the undamaged and damaged states are compared to detect the damage of shear connectors. Sensors are placed on top of the slab to measure the vertical responses of the slab, and underneath the corresponding girder location to record the vertical responses of the girder.

The damage index is defined as the relative difference between PSDT vectors in the undamaged and damaged states

$$DI(PSDT_{ud}(\omega), PSDT_d(\omega)) = \frac{\|\{PSDT_{ud}(\omega)\} - \{PSDT_d(\omega)\}\|}{\|\{PSDT_{ud}(\omega)\} + \{PSDT_d(\omega)\}\|} \quad (13)$$

where $PSDT_{ud}(\omega)$ and $PSDT_d(\omega)$ are PSDT vectors from the slab response to the girder response in the undamaged and damaged states, respectively. They are

$$\begin{cases} PSDT_{ud}(\omega) = \frac{|H_{ud}^g(\omega)|^2}{|H_{ud}^s(\omega)|^2} \\ PSDT_d(\omega) = \frac{|H_d^g(\omega)|^2}{|H_d^s(\omega)|^2} \end{cases} \quad (14)$$

in which, $H_{ud}^g(\omega)$ and $H_{ud}^s(\omega)$ are the FRFs corresponding to sensor locations on the girder and slab in the undamaged state, respectively; $H_d^g(\omega)$ and $H_d^s(\omega)$ are the FRFs corresponding to the girder and slab sensor locations in the damaged state, respectively.

A high damage index value denotes a significant difference in PSDT between the slab and girder responses at a specific location and indicates the existence of damage in shear connectors around this area. The reason that the local PSDT is selected for condition assessment of shear connectors is that it would change significantly as the loading transfer path from the slab to the girder varies due to the damage of shear connectors. It should be noted that the frequency response functions at slab and girder locations are obtained by the experimental modal analysis with the measured input and acceleration responses. The PSDT vectors in the undamaged and damaged states can be calculated with Eq. (14), and the damage index could be obtained from Eq. (13). The proposed damage detection method is cataloged as the non-model based method as the finite element model of the structure is not required in the identification.

3.4 Case 2: damage detection without measured data from undamaged structure

In this case, only the measured responses from the damaged structure are used for the identification. To identify the shear connector damage, a reference sensor is defined to compute the PSDT vectors from the reference sensor location to a slab sensor location and the corresponding

girder sensor location, respectively. These PSDT vectors can be expressed as

$$\begin{cases} PSDT_{sr}(\omega) = \frac{|H_d^s(\omega)|^2}{|H_d^r(\omega)|^2} \\ PSDT_{gr}(\omega) = \frac{|H_d^g(\omega)|^2}{|H_d^r(\omega)|^2} \end{cases} \quad (15)$$

in which, $H_d^r(\omega)$ is the FRF at the reference sensor location in the damaged state. $H_d^s(\omega)$ and $H_d^g(\omega)$ are the FRFs corresponding to sensor locations on the slab and girder in the damaged state, respectively.

If damages of shear connectors exist, FRF at the slab sensor location $H_{ad}^s(\omega)$ will not be exactly the same as that at the girder sensor location $H_{ad}^g(\omega)$. Therefore, $PSDT_{sr}(\omega)$ will not be exactly the same as $PSDT_{gr}(\omega)$. A damage index is then defined based on this fact to identify the damage of shear connectors as follows

$$DI(PSDT_{sr}(\omega), PSDT_{gr}(\omega)) = \frac{\| \{PSDT_{sr}(\omega)\} - \{PSDT_{gr}(\omega)\} \|}{\| \{PSDT_{sr}(\omega)\} + \{PSDT_{gr}(\omega)\} \|} \quad (16)$$

A high damage index value in Eq. (16) indicates the significant difference between two PSDT vectors and the existence of damage of shear connector in the nearby area.

3.5 Establishment of a threshold value for damage detection

When n damage indices are obtained at different sensor locations, the mean value and standard deviation of these damage indices can be computed and expressed as μ and σ . The one-side upper confidence limit for the damage index can be defined as (Ross 2004)

$$UL = \mu + Z_\alpha \times \frac{\sigma}{\sqrt{n}} \quad (17)$$

where Z_α is the value of a standard norm distribution with zero mean and unit standard deviation such that the cumulative probability is $100 \times (1 - \alpha)\%$. The upper confidence limit UL is considered as a threshold value to indicate possible abnormalities in the damage index. The definition of this threshold value is based on the statistical properties of the calculated damage indices. Damage index values which are larger than the threshold value indicate possible damages existence. Others smaller than the threshold value are identified as undamaged. This statistical definition of a threshold value is also adopted in Ren *et al.* (2008). With consideration of the threshold value, a new damage indicator ($DI - UL$) is used in this study to identify damage, in which DI is the damage index obtained from Eqs. (13) or (16). It should be noted that the undamaged locations are determined when the damage index value DI is less than the threshold value. To highlight the detected damage locations, the values of ($DI - UL$) on undamaged locations are taken as zeros and other positive values of ($DI - UL$) on possibly damaged locations will be shown.

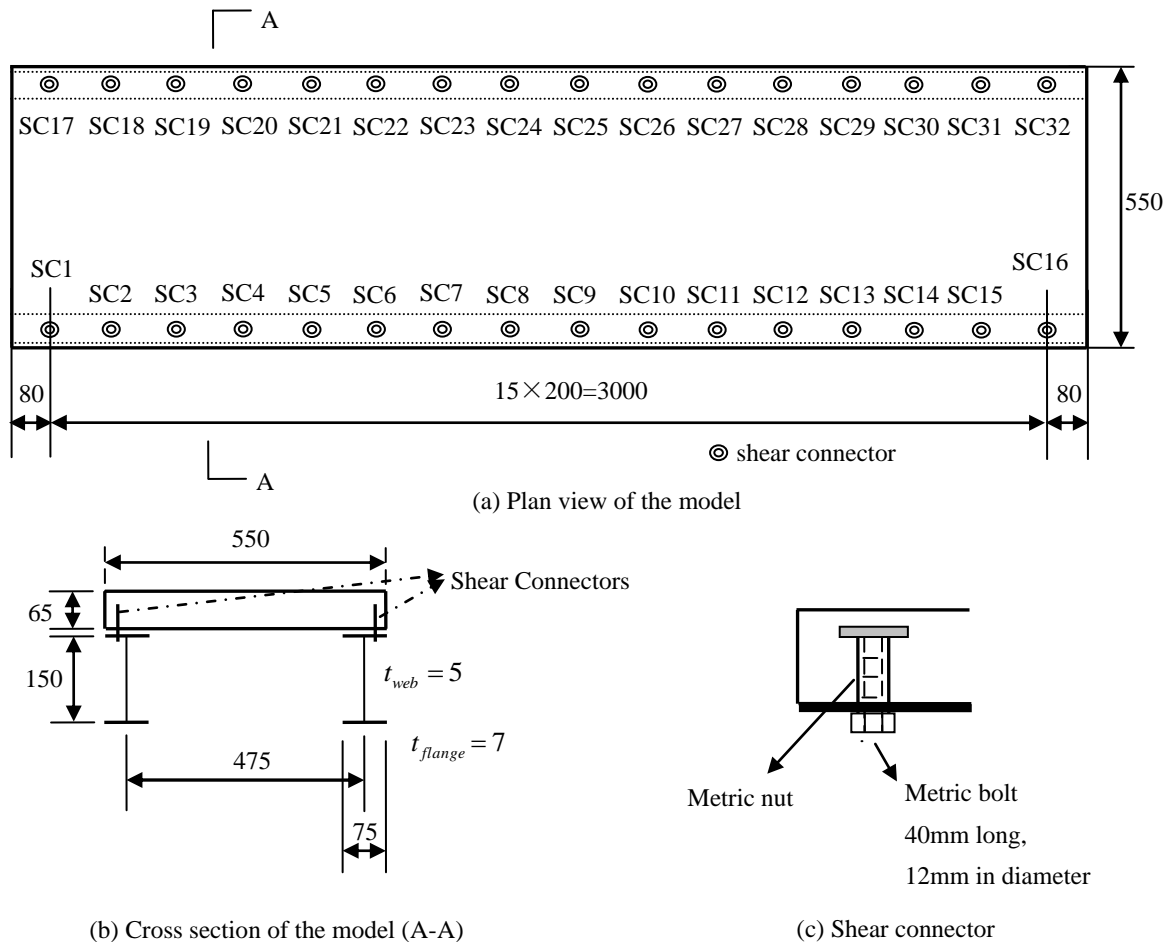


Fig. 1 Dimensions and shear connector details of the slab-on-girder structure (unit: mm)

4. Numerical studies

Numerical studies on a simply-supported slab-on-girder bridge structure are conducted to illustrate the accuracy and efficiency of the proposed approach for damage detection of shear connectors. Fig. 1 shows the plan view and cross section of the structure and details of a shear connector. The concrete slab is supported on two steel I-type girders, and shear connectors are used to link the slab and girders together. Each girder has sixteen shear connectors with equal space and there are thirty-two shear connectors in total in the structure. They are denoted as SC1~SC32 in Fig. 1(a). The cross-section of the structure is shown in Fig. 1(b). To be consistent with the laboratory tests that will be described later, the shear connector is simulated as a metric bolt screwing into a metal nut, as shown in Fig. 1(c). The shear link fixity is provided by securing the metric bolt. The failure of bolts will cause the shear slippage between the slab and girder and reduce the load-carrying capacity of composite bridges. In this study, the bolt is fully unscrewed from the metal nut to simulate the failure of shear link.

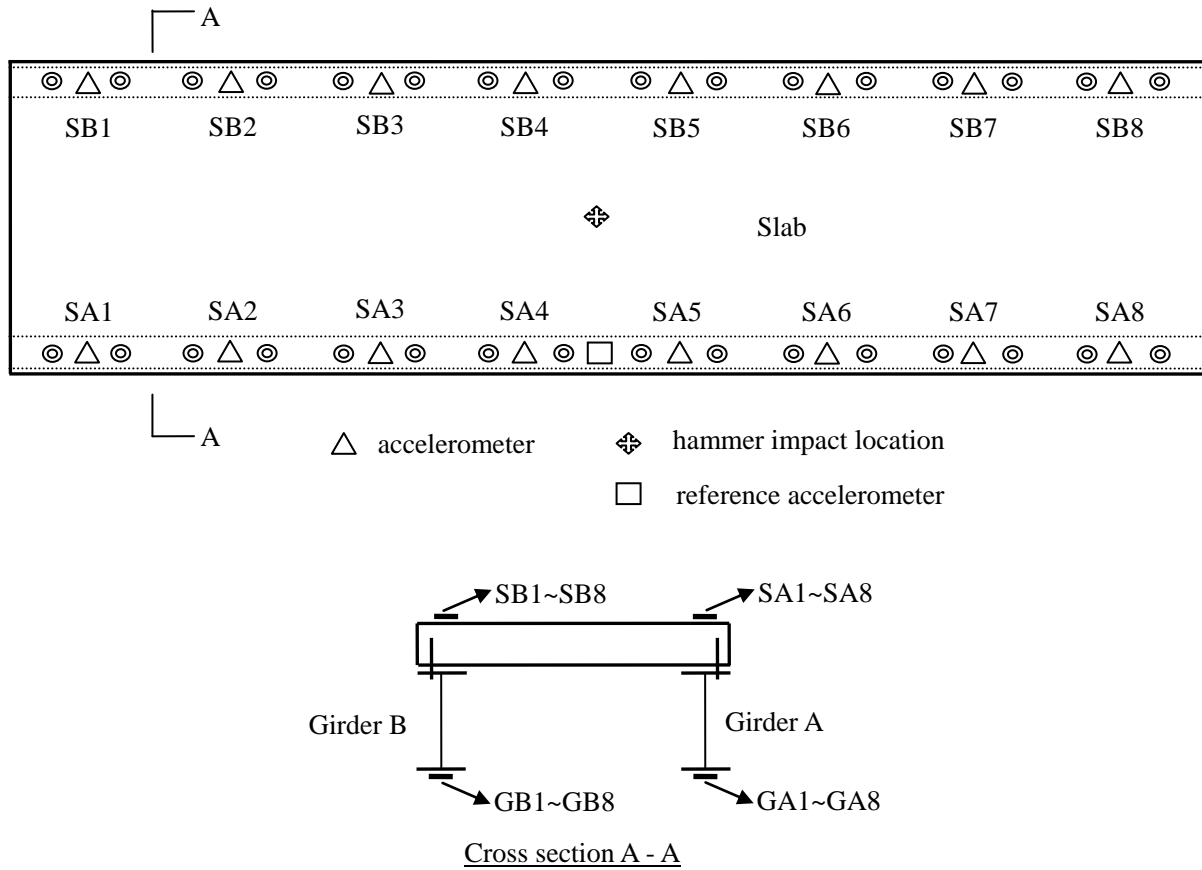


Fig. 2 Sensor locations on the slab and underneath the girders

4.1 Finite element model and sensor placement configuration

Slab and steel girders are modeled with shell elements, and shear connectors are modeled with beam elements (Xia *et al.* 2008) that link the slab and girders. The axial stiffness and shear stiffness of a shear connector are obtained by the formulas from an existing study (Chiewanichakorn *et al.* 2004). The finite element model of the slab-on-girder structure consists of 695 nodes, 600 shell elements and 32 beam elements. Each node has six DOFs and the system has 4170 DOFs in total. The Young's modulus and mass density of slab concrete are 3.18×10^4 MPa and 2500 kg/m^3 , respectively. The Young's modulus and mass density of steel girder are 2×10^5 MPa and 8092 kg/m^3 , respectively. The first three natural frequencies in the vertical direction are calculated as 35.9Hz, 113.96Hz and 144.96Hz, respectively. Rayleigh damping is assumed and the damping ratios for the first two modes are taken as $\zeta=0.012$ in the simulation.

Fig. 2 shows the locations of accelerometers placed on the slab, denoted as "SA1-SA8" and "SB1-SB8", and those underneath the girders, denoted as "GA1-GA8" and "GB1-GB8", for measurement of the acceleration responses under impact tests. Responses at these sensor locations are numerically calculated by applying an impact force. 8192 points of measured input and

Table 1 Damage scenarios in numerical study

Damage Scenario	Shear connectors removed
Scenario 1	SC9, SC10, SC25 and SC26
Scenario 2	SC1, SC2, SC15 and SC16

Table 2 Identified frequencies of the undamaged and damaged structures in numerical study

Mode	Undamaged (Hz)	Damage Scenario 1 (Hz)	Change (%)	Damage Scenario 2 (Hz)	Change (%)
1	35.74	35.55	0.53	33.78	5.48
2	109.94	106.42	3.2	101.27	7.89
3	144.76	143.13	1.13	142.77	1.37
4	233.5	228.9	1.97	202.91	13.1

Table 3 MAC values of the damaged structure in numerical study

Mode	Damage Scenario 1	Damage Scenario 2
1	1.000	0.96
2	0.999	0.63
3	0.992	0.59
4	0.940	0.36

response data with a sampling rate of 1000Hz are used in numerical simulations. The calculated acceleration responses are analyzed to extract the vibration properties of the structure and to derive the FRF with DIAMOND toolbox. Two damage scenarios are assumed, as shown in Table 1. Damages of shear connectors are simulated by removing the specific shear links (represented by beam elements in the finite element model). As the numerical simulation is rather standard, it is not described here in detail.

To simulate the effect of measurement noise, a normally distributed random noise with zero mean and unit standard deviation is added to the calculated dynamic response as

$$\ddot{x}_n = \ddot{x}_{cal} + E_p N_{oise} std(\ddot{x}_{cal}) \quad (18)$$

where \ddot{x}_n and \ddot{x}_{cal} are the simulated response with noise effect and the original calculated response, respectively; E_p is the noise level and equals to 0.03 if 3% noise is included in the response; N_{oise} is a standard normal distribution vector with zero mean and unit standard deviation and $std(\ddot{x}_{cal})$ denotes the standard deviation of the original calculated response. Two noise levels, namely 3% and 5%, are included in the simulated “measured” acceleration responses and 1% in the input force in this study.

4.2 Modal identification results

The first four vertical frequencies and the associated mode shapes of the structure in the undamaged and damaged states are identified and the modal frequencies are shown in Table 2. Modal Assurance Criterion (MAC) values of these four mode shapes at the slab sensor locations of

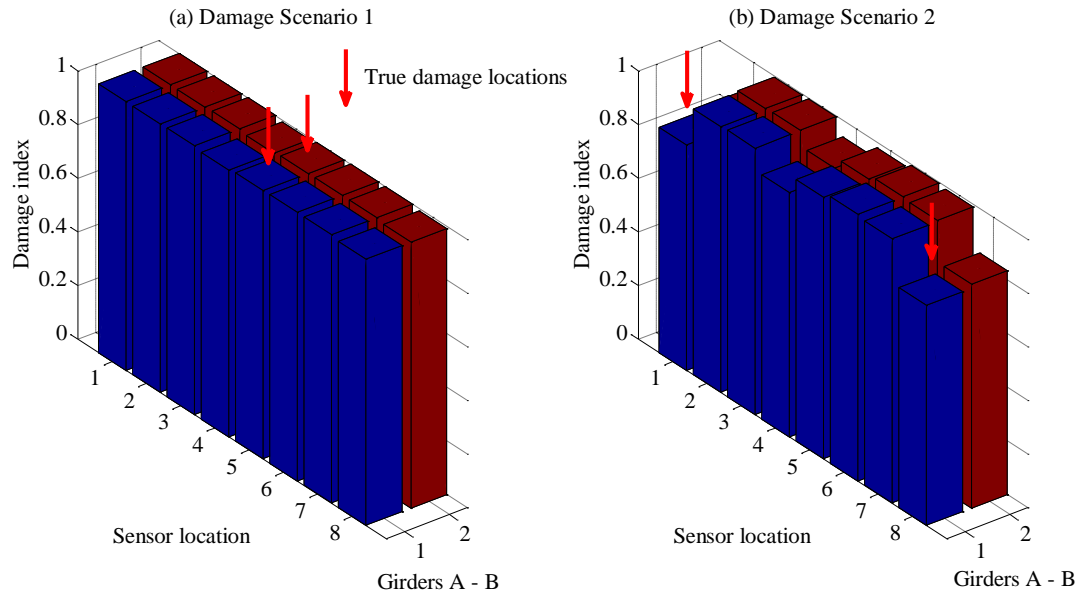


Fig. 3 Damage detection results with COMAC

two damage scenarios are shown in Table 3. It can be seen that the changes of frequencies are not prominent in damage Scenario 1. The largest one is 3.2% in the second frequency. This small frequency change of less than 5% indicates it could be difficult for confident damage identification with only vibration frequencies. For the damage Scenario 2, the change of the first frequency is 5.48% and it increases to 13.1% at the fourth frequency with a MAC value of 0.36. It is noted that the MAC value of the second mode from damage Scenario 2 is quite low as 0.63 this is because no diaphragm is placed at support locations and the introduced damages in Scenario 2 significantly affect the second identified mode shape. These significant changes indicate the damage existence could be confidently identified with global modal information. However, the damage location cannot be identified without performing further analysis such as model correlation and updating.

4.3 Case A: measured data from undamaged model available

In this case, measured acceleration response data and hammer impact force from the structure in both the undamaged and damaged states are measured to identify the modal information and derive the FRF at each sensor location for the computation of PSDT.

4.3.1 Damage detection with global modal information

Damage detection results with COMAC based on the identified four mode shapes are shown in Fig. 3. It can be seen that COMAC fails to identify the damages in Scenario 1 as no obvious reductions in COMAC values are observed at the sensor location No. 5 in both girders. For Scenario 2, COMAC can identify the damages in sensor locations No. 1 and No. 8 of Girder A. However, two false identifications are detected at sensor locations No. 1 and No. 8 of Girder B as they are close to the true damages, and two more false identifications at sensor location No. 4 in both girders. Fig. 4 shows the damage detection results with changes in flexibility. It can be found

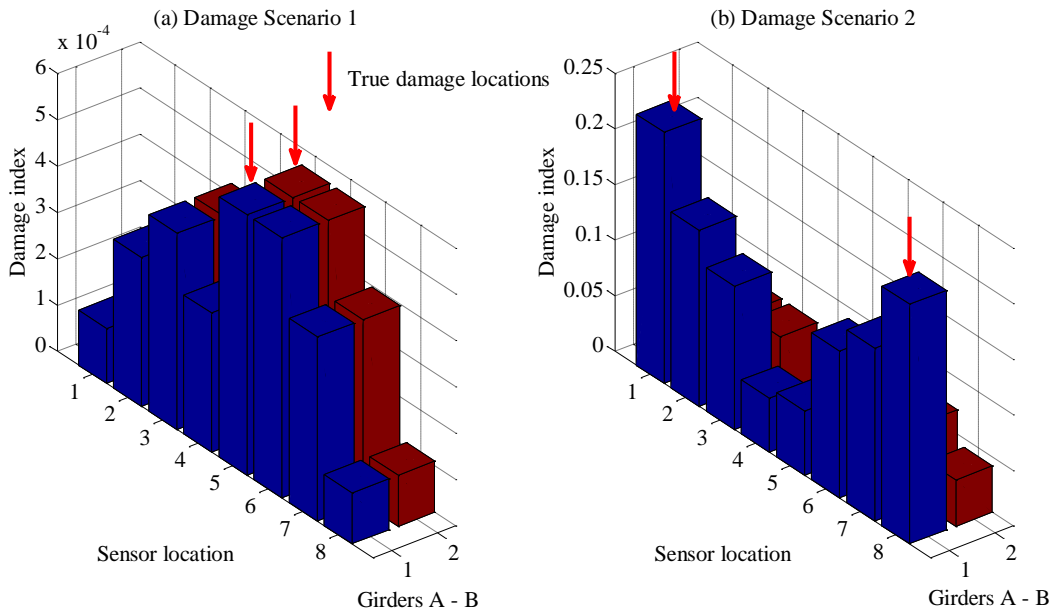


Fig. 4 Damage detection results with changes in flexibility

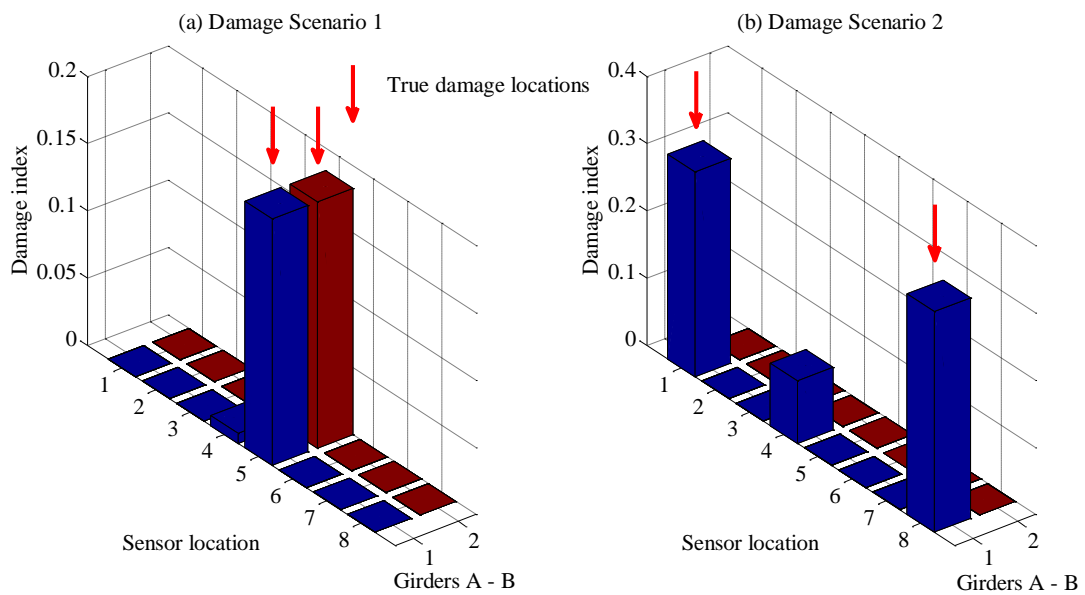


Fig. 5 Damage detection results using PSDT with data from undamaged structure available (no noise)

that the damages in sensor location No.5 of Scenario 1 can be detected, while two false identifications are observed at sensor location No. 6 in both girders as they are near the true damage locations. The damages in Scenario 2 are identified accurately indicating that the detection using changes in flexibility is more sensitive than COMAC.

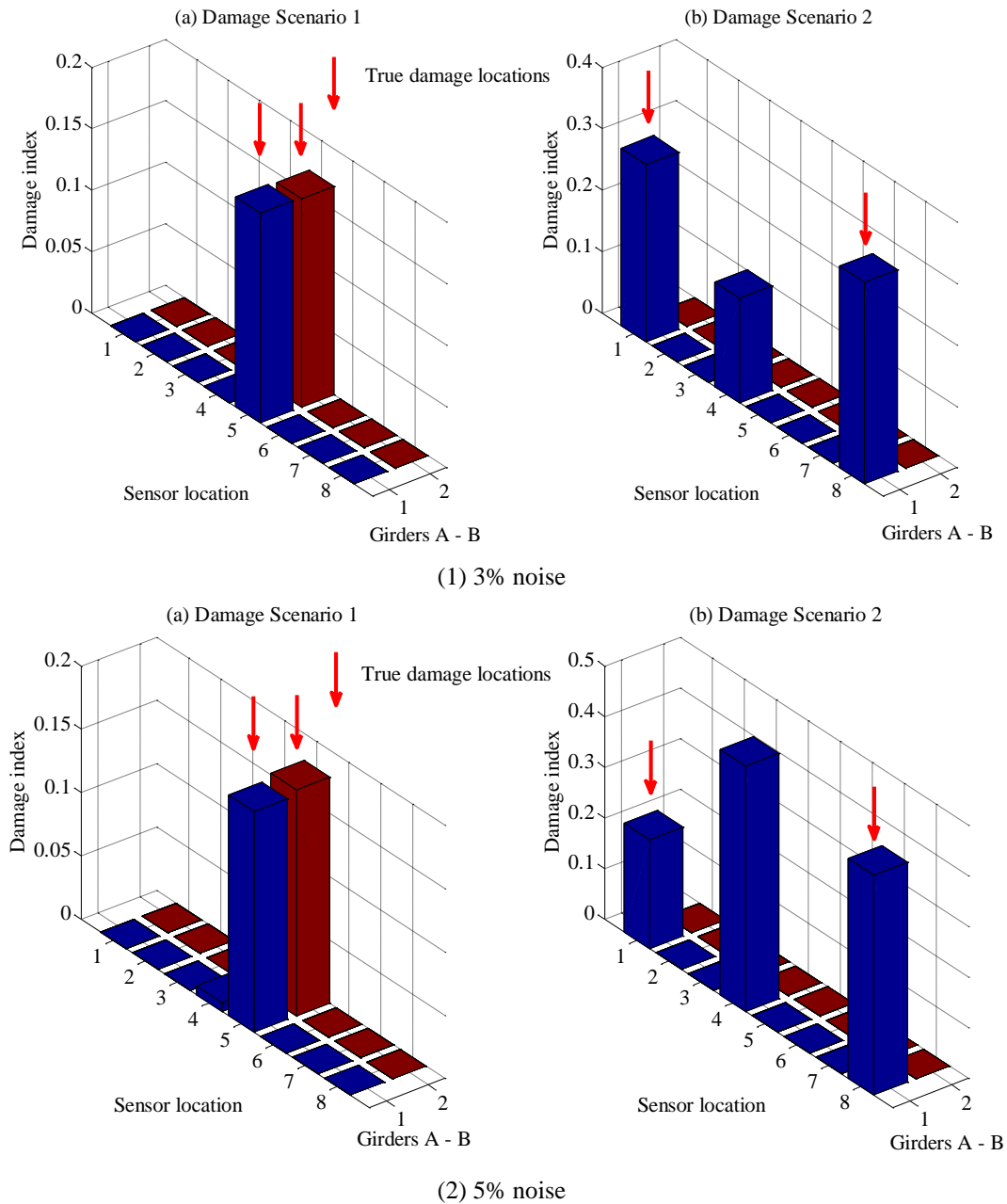


Fig. 6 Damage detection results using PSDT with data from undamaged structure available (with noise)

4.3.2 Damage detection with power spectral density transmissibility

PSDT vectors in the frequency range of 25~115 Hz in the undamaged and damaged states are compared to compute the damage index with Eq. (13). This frequency range covering only the first two modes is defined to investigate the reliability and robustness of the proposed damage detection approach. The determination of the selected frequency range is based on covering the most reliably

identified mode shapes and avoiding the oscillation frequency band due to the initialization process. α is set to be 0.02 in Eq. (17) to obtain the upper confidence limit and then compute the new damage indicator ($DI-UL$) with consideration of this threshold value. Fig. 5 shows the damage detection results of two damage scenarios from measurements without noise effect. Identified results of Scenario 1 for Girders A and B are shown in Fig. 5(a). It can be clearly seen that high damage indices at the sensor location No. 5 in both girders are observed. The damage index is around 0.2, indicating the simulated damage locations are identified correctly. Fig. 5(b) shows the detection results of Scenario 2 in Girders A and B. It can be seen that damage index values at sensor location No. 1 and No. 8 in Girder A are around 0.3, indicating the existence of damage of shear connectors in these sensor locations. These identified locations match well with the introduced damage locations. However, it should be noted in Fig. 5 that damage index values corresponding to the two damage scenarios at sensor location No. 4 in Girder A where there is no shear connector damage are also relatively high, implying false damage identification. This is because the response at the mid span of the simply-supported model is the largest. Because the steel girder and concrete slab in the current structure model are only connected by 16 shear connectors between each girder and slab, some different responses between slab and girder is expected, and which is most significant when the response is relatively large at the mid span. This response difference is also picked up by the proposed damage index.

Fig. 6 shows the detection results from the simulated responses with smeared noise. The damage index values in Scenario 1 at the sensor location No. 5 in both girders are around 0.2 with two noise levels considered in the study, indicating the damage locations of shear connectors are identified accurately. Damage index values in Scenario 2 at sensor locations No. 1 and No. 8 in Girder A are greater than 0.2 for both the noise level cases, indicating again that the true damage location is successfully identified. However, similar to the observations from Fig. 3, a false identification at sensor location No. 4 in Girder A exists. In damage Scenario 2, the falsely identified damage index at this location increases with the noise level and is up to 0.4 with 5% noise.

Detection results with COMAC and changes in flexibility shown in Figs. 3 and 4 demonstrate that using global modal information may not correctly identify the damages of shear connectors in minor damage case with very small frequency and MAC changes. The proposed local dynamic condition assessment approach can successfully identify the shear connector damage locations in two damage scenarios and shows the advantages over the traditional detection method based on global modal information with more accurate results and less false identifications. A few false identifications occur at the mid span owing to relatively large displacement response at this location since the steel girders and concrete slab are not continuously connected together in the model considered in this study. This false identification might become more prominent when the simulated data are smeared with 5% noise.

4.4 Case B: measured responses from undamaged model not available

This section demonstrates shear connector damage identification using only the measured responses from the damaged structure.

4.4.1 Damage detection with relative difference of frequency response functions

The relative difference between FRFs on the slab and corresponding girder location is used to detect the damage locations of shear connectors (Xia *et al.* 2008). Only the measured response data

and hammer impact force from the structure in the damaged state are required to extract the FRFs for identification. Figs. 7 and 8 show the damage detection results based on the relative difference of FRFs without and with noise effect, respectively. The introduced damages are identified correctly with several false identifications close to the true damage locations, such as sensor

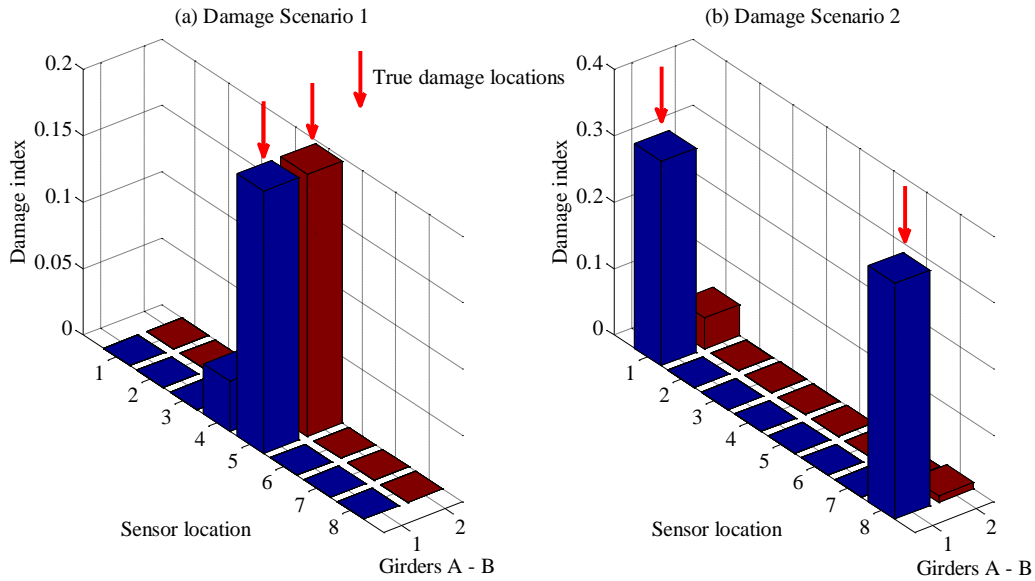
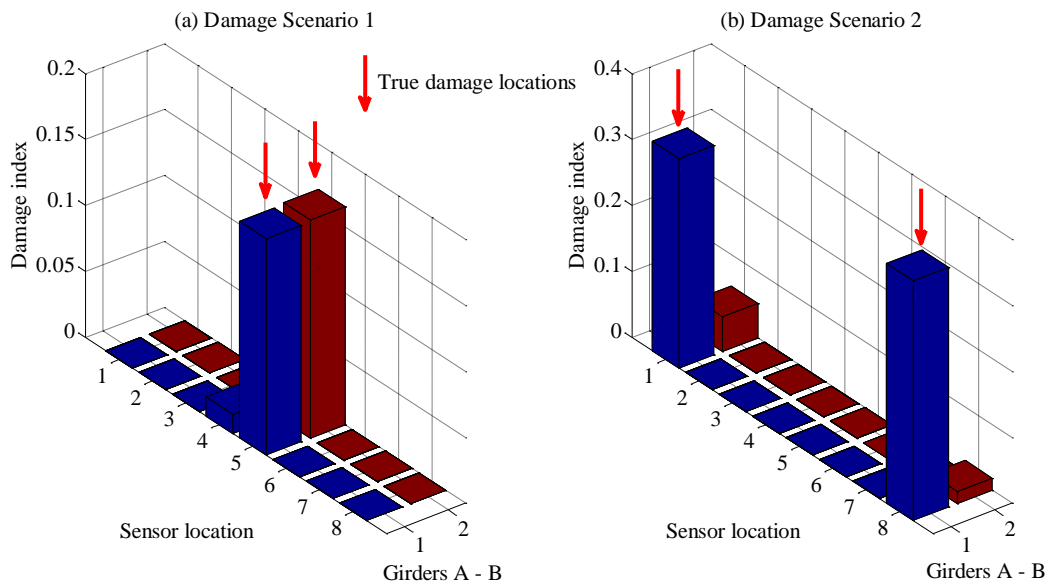
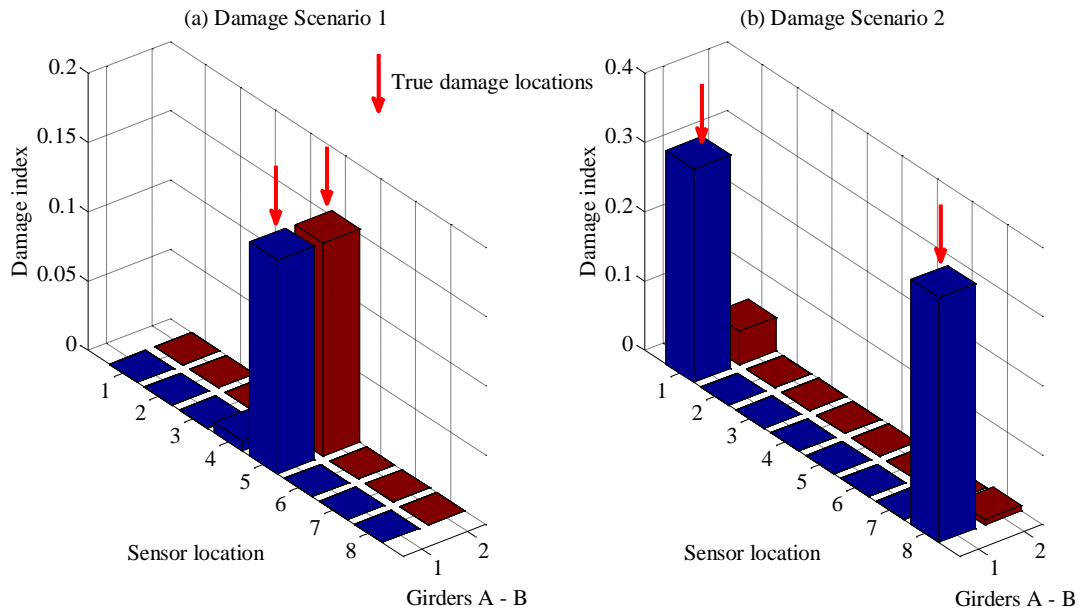


Fig. 7 Damage detection results using RDFRF without data from the undamaged structure (no noise)



(1) 3% noise

Fig. 8 Damage detection results using RDFRF without the data from the undamaged structure (with noise)



(2) 5% noise

Fig. 8 Continued

location No.4 of Girder A in Scenario 1 and sensor locations No. 1 and No. 8 of Girder B in Scenario 2.

4.4.2 Damage detection with power spectral density transmissibility

As discussed above, when the measured data of undamaged structure are not available, a reference measurement is obtained to compute the PSDT from the reference response to those measured on slab and on girder locations for damage identification. The reference sensor location is thus included in the sensor placement configuration of the above studies. It is placed on the central slab location on the top of Girder A, as shown in Fig. 2. Other sensor locations stay unchanged. PSDT vectors from the reference sensor response to the slab and girder responses are obtained with Eq. (15), and PSDT vectors in the frequency range of 25~115 Hz are used to compute the damage index from Eq. (16). α is set to be 0.02 to calculate the threshold value with Eq. (17). Figs. 9(a) and 9(b) show the identified results from the measured responses without noise for damage Scenarios 1 and 2, respectively. It can be clearly seen that the introduced damages of shear connectors at the sensor location No.5 in two girders are identified accurately in Scenario 1. A false identification is observed at the sensor location No. 4 in Girder A. For Scenario 2, the introduced shear link damages are close to sensor locations No. 1 and No. 8 in Girder A and are detected accurately. A small false positive is found at sensor location No. 8 in Girder B. False identifications exist in these two scenarios from measured responses without noise effect due to the smearing effect as they are close to the true damage locations. It is interesting to note that the false identification at the mid span does not appear in this case in damage Scenario 2. This is because the reference point used in calculating PSDT is located at the mid span of the girder A, which effectively eliminates the false identification at this location.

Fig. 10 shows the damage detection results from simulated responses with two noise levels. The identified results demonstrate that the locations of damages in both scenarios are detected accurately. The damage index values in Scenario 1 at sensor location No. 5 in both girders are

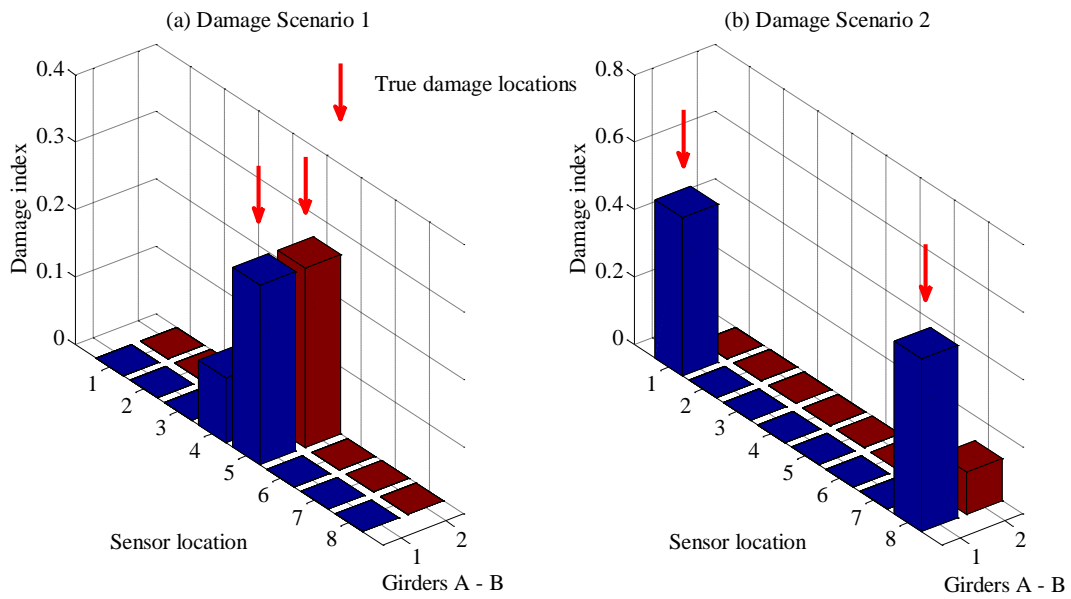
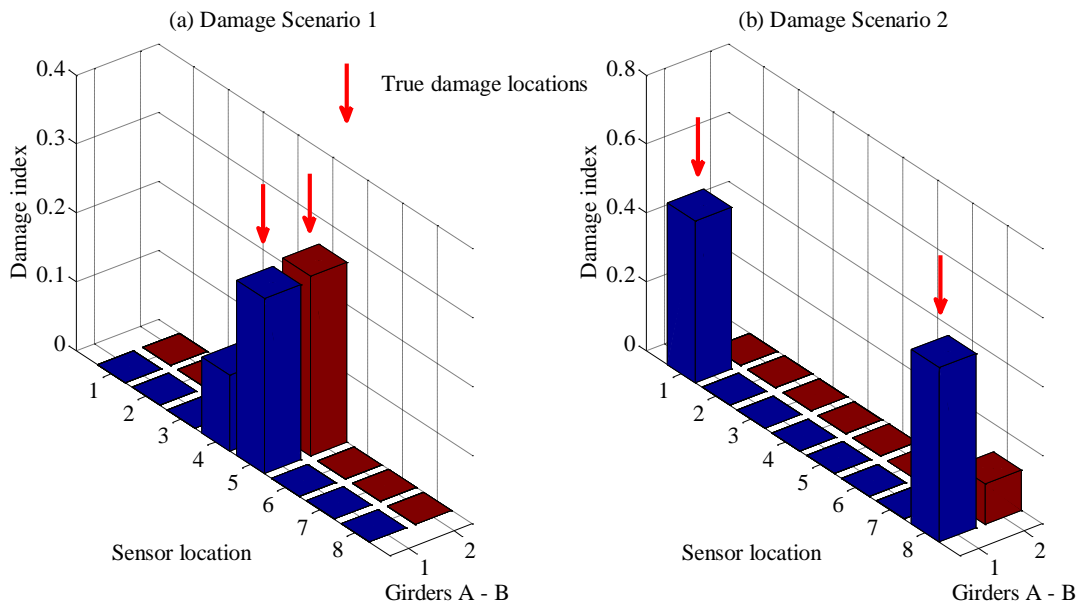
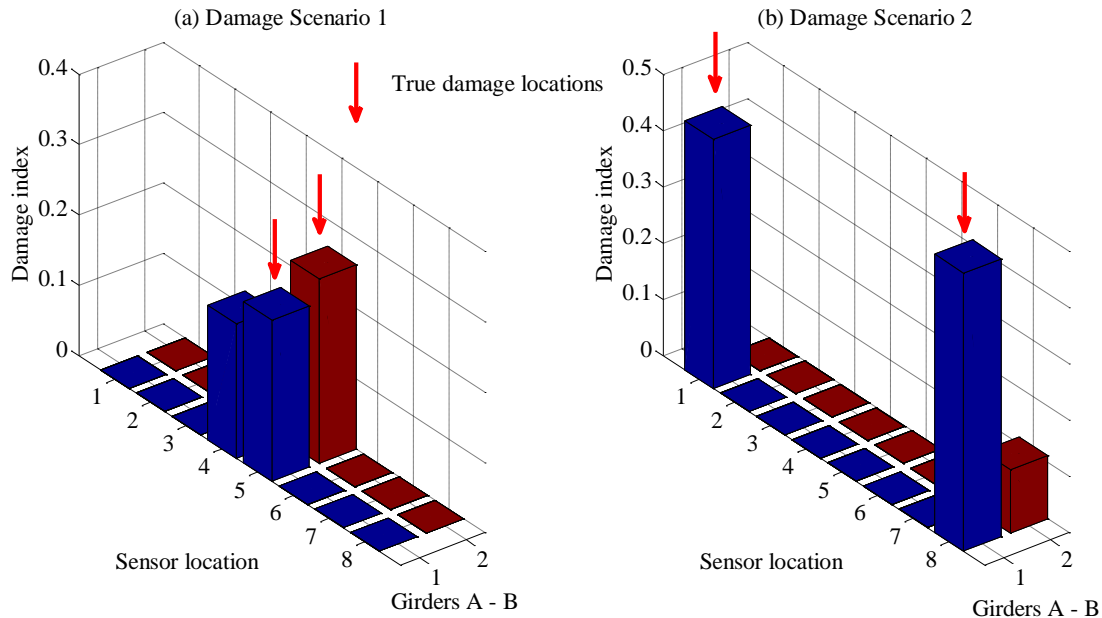


Fig. 9 Damage detection results using PSDT with data from undamaged structure unavailable (No noise)



(1) 3% noise

Fig. 10 Damage detection results using PSDT with data from undamaged structure unavailable (with noise)



(2) 5% noise

Fig. 10 Continued

around 0.25 in two noise level cases. The identified damage indices in Scenario 2 at sensor location No. 1 and No. 8 in Girder A are around 0.4. Several false identifications, such as sensor location No. 4 of Girder A in Scenario 1 and sensor location No. 8 of Girder B in Scenario 2, are observed. It should be noted that the damage index value at sensor location No. 4 in Girder A of Scenario 1 increases to 0.15 when the 5% noise is smeared in the responses.

Compared with the detection results shown in Figs. 7 and 8, it can be found that the damage indices calculated from the proposed method with PSDT are generally larger than those from the relative difference of FRFs. It may indicate that the proposed condition assessment method has a higher sensitivity to detect the damage however a false identification is observed in the results with the proposed approach. The robustness of the proposed approach for damage detection of shear connectors from noisy measurements is demonstrated.

5. Experimental studies

5.1 Introduction and experimental setup

Experimental studies are conducted to validate the proposed damage detection approach. A slab-on-girder structure is fabricated and tested in the laboratory. The measured hammer impact force and acceleration responses are used for the damage detection. The performance of the proposed approach for identification of shear connector conditions is investigated.

The testing model was constructed with a concrete slab supported on two steel girders. Sixteen shear connectors were mounted with equal space in each girder to link the slab and steel girder



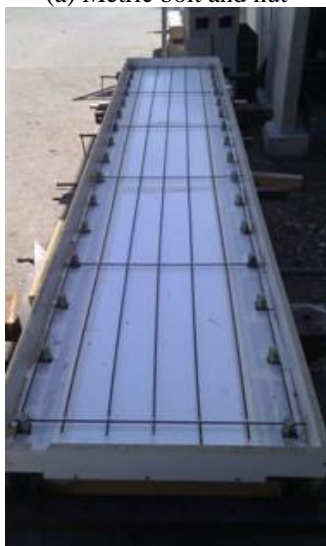
Fig. 11 Experimental setup of the slab-on-girder structure



(a) Metric bolt and nut



(b) Bolt screwed into the nut



(c) Plan view of shear connectors



(d) Shear connector in the structure

Fig. 12 Design of shear connectors

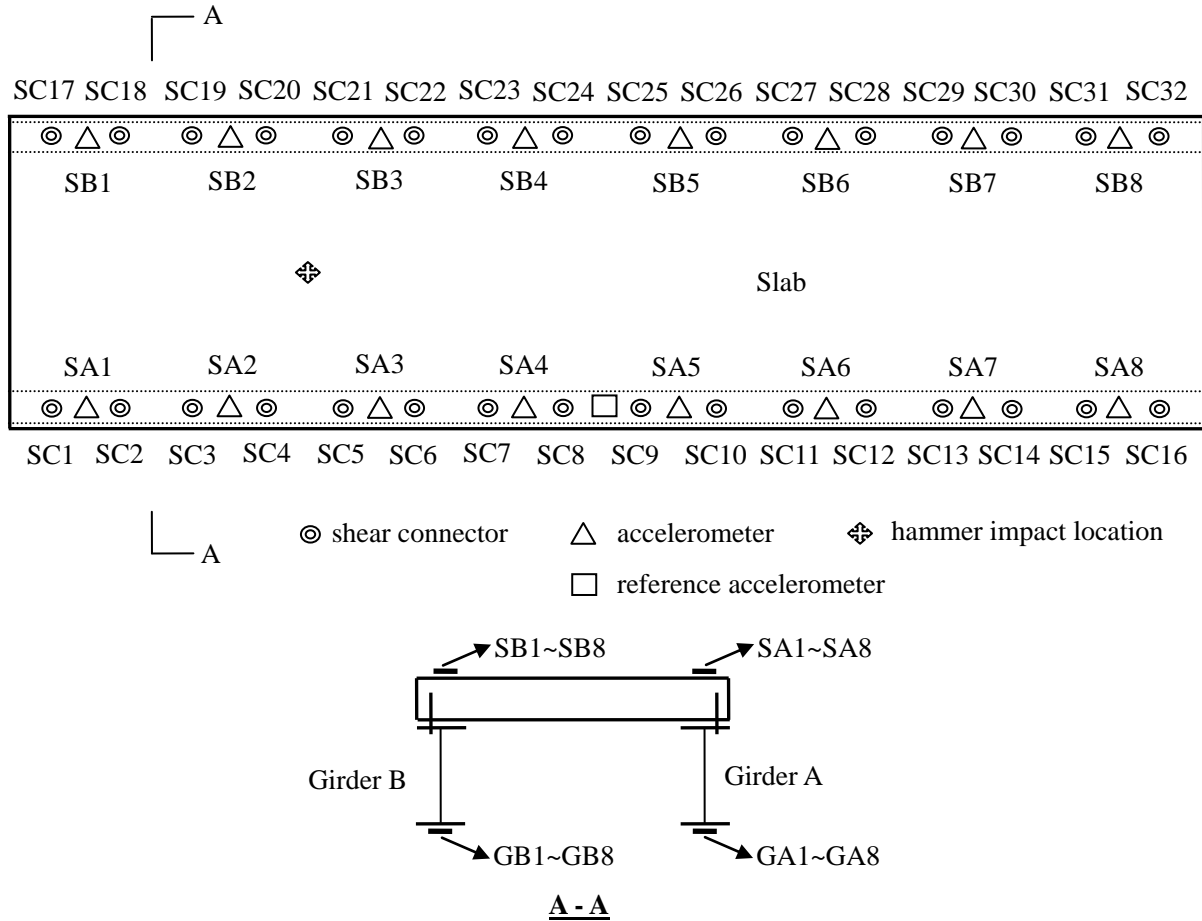


Fig. 13 Experimental sensor placement

together. It was located on two steel frames which were fixed on the strong ground as shown in Fig. 11. The design of shear connectors considers the ability not only to simulate failure of specific shear links, but also to reset-up them to the undamaged state. Therefore, a metric bolt screwing into a metric nut casted in the slab was used to connect the slab and girder. The metric nuts were welded onto the reinforcement bar in the slab before pouring. Design and setup of shear connectors can be seen in Fig. 12. If all the bolts are screwed into their nuts, the structure condition corresponds to the undamaged state. The damage of shear connectors is introduced into the structure by fully unscrewing several specific metric bolts to simulate the failure of shear links. The dimensions of the laboratory model are the same as those of the model in the numerical study. It should be noted that the proposed damage detection approach for shear connectors is non-model based as the finite element model of the structure is not required. Therefore the dimensions, boundary conditions of the model and material properties of the slab, girder and shear connectors are not introduced because they are not required for damage identification.

Nine Kistler 8330A3 accelerometers were used in the laboratory dynamic tests to collect the acceleration responses of the structure. An instrumented 5820A sledge hammer with a rubber tip

Table 4 Damage scenarios in experimental study

Damage Scenario	Shear connectors removed
Scenario 1	SC7, SC8, SC23 and SC24
Scenario 2	SC1, SC2, SC15 and SC16

Table 5 Identified frequencies of the undamaged and damaged structures in experimental study

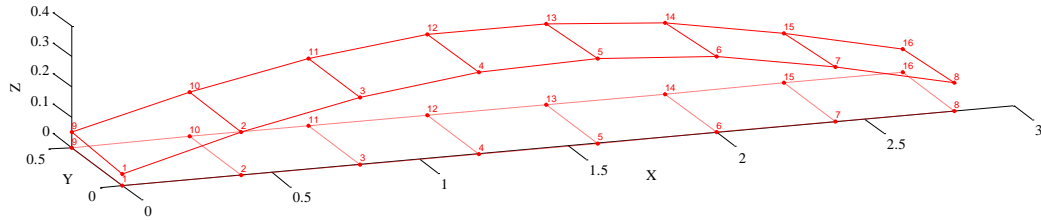
Mode	Undamaged (Hz)	Damage Scenario 1 (Hz)	Change (%)	Damage Scenario 2 (Hz)	Change (%)
1	41.27	41.12	0.36	38.05	7.80
2	116.61	116.52	0.08	100.35	13.94
3	265.54	263.37	0.82	220.19	17.08

was used to generate the impact excitation. A sixteen-channel conditioner and data acquisition system was employed to record the hammer force and acceleration signals. The recording sampling frequency was set as 2000Hz. DIAMOND data analyzing toolbox was employed to conduct the experimental modal analysis and calculate the FRF at each sensor location.

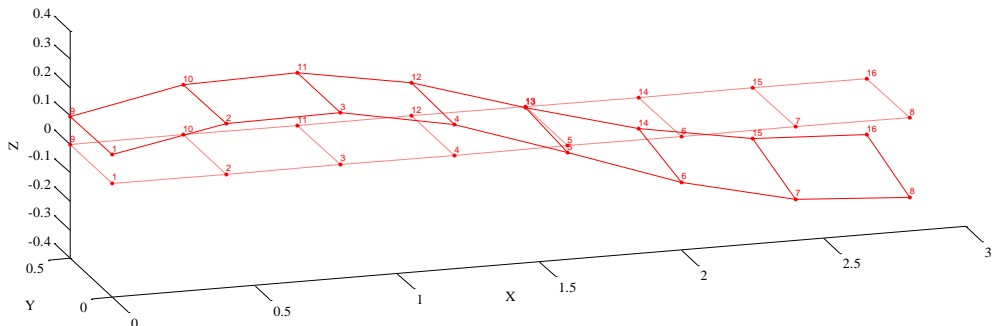
Fig. 13 shows the numbering of shear connectors and sensor locations defined in the tests. Each girder has sixteen shear connectors linking the concrete slab and steel girder together and one sensor is located at the center of two shear connectors. A sensor is placed at the central slab on the top of Girder A as the reference sensor and its location stays unchanged during the testing. Other eight sensors were repeatedly placed on the slab or underneath the girders to measure the responses at sensor locations SA1~SA8, SB1~SB8, GA1~GA8 and GB1~GB8. It is noted that the number of sensors is not a significant factor to perform the proposed damage detection approach since repeated tests with those movable sensors would measure a number of responses at different locations. Two damage scenarios are listed in Table 4. Excitation with hammer impact was applied at the left quarter span of the slab as shown in Fig. 13.

5.2 Identified frequencies and mode shapes

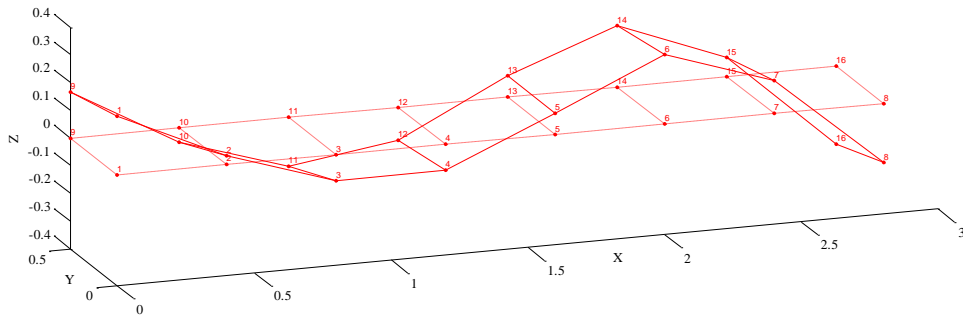
The first three identified natural frequencies of the undamaged and damaged structures are listed in Table 5. Fig. 14 shows the corresponding identified mode shapes of the undamaged structure. The identified mode shapes of the damaged structure are similar and therefore are not shown here. MAC values at the slab sensor locations of two damage states are shown in Table 6. It can be seen from Table 5 that minor changes of the first three frequencies are observed in damage Scenario 1. The largest one is only 0.82% at the third frequency, and its corresponding MAC value is 0.923. Therefore it will be difficult to confidently identify the damage of shear connectors with the changes of frequencies and mode shapes. For the damage Scenario 2, the largest change of natural frequency is 17.08% at the third mode, and its MAC value is 0.449. This observation is consistent with that in the numerical study. Since this structure has no diaphragms at two ends, the damage of shear connectors at support locations induces large changes of frequencies and MAC values. Table 7 shows the comparison between the natural frequencies of experimental and numerical models. The differences come from the model errors, such as in the materials properties and boundary conditions. If model-based damage detection approaches are employed, initial finite element model updating has to be conducted to adjust the numerical model.



(1) First mode



(2) Second mode



(3) Third mode

Fig. 14 Identified first three mode shapes of the undamaged structure

Table 6 MAC values of the damaged structure in experimental study

Mode	Damage Scenario 1	Damage Scenario 2
1	1.000	0.984
2	0.999	0.898
3	0.923	0.449

Table 7 Natural frequencies of experimental and numerical models

Mode	Frequencies (Hz)		Difference (%)
	Experimental model	Numerical model	
1	41.27	35.74	13.4
2	116.61	109.94	5.72
3	265.54	233.5	12.07

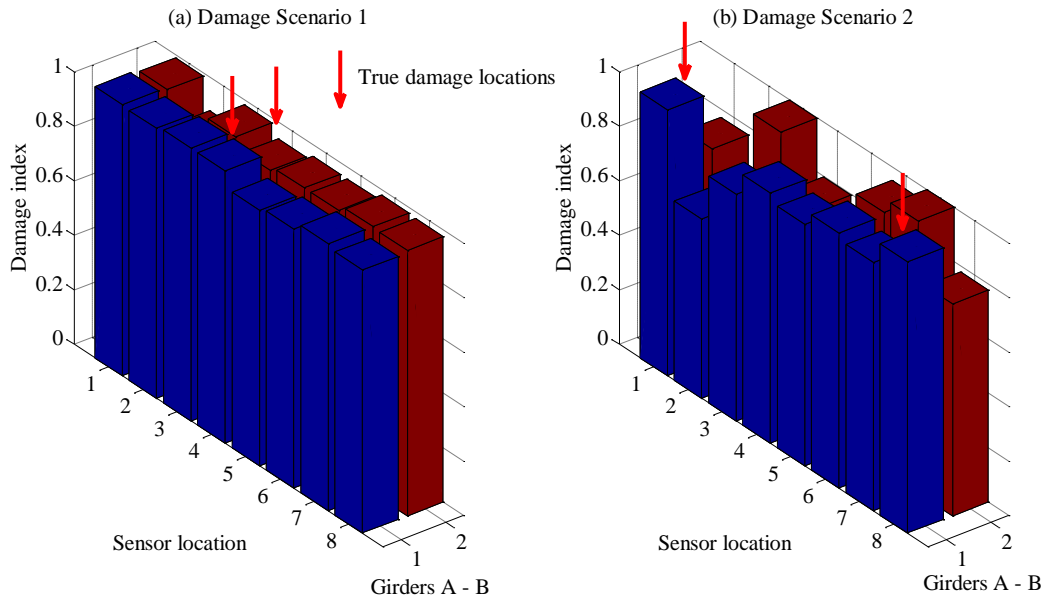


Fig. 15 Damage detection results with COMAC

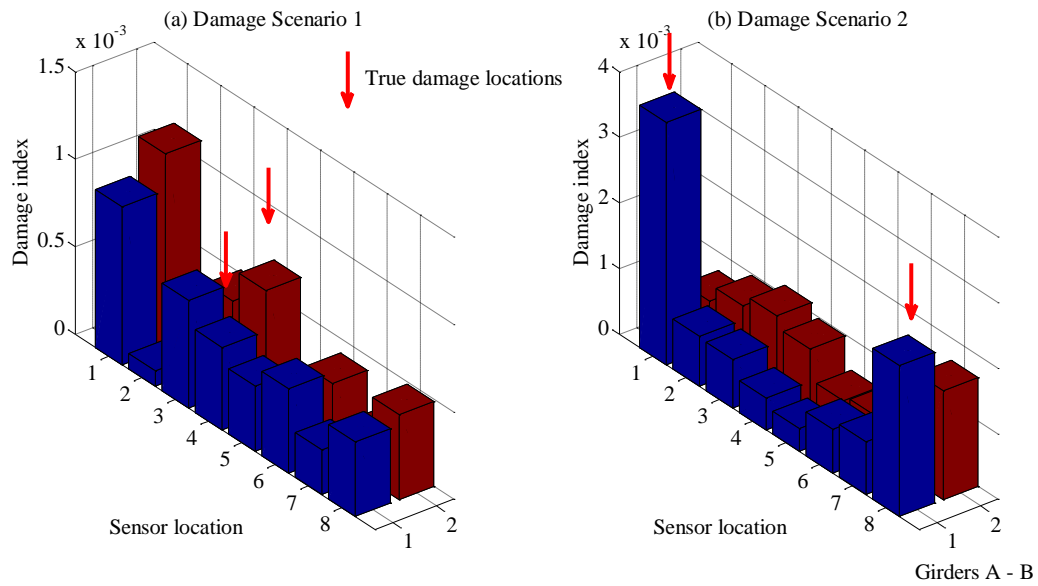


Fig. 16 Damage detection results with changes in flexibility

5.3 Case A: measured data from undamaged model available

5.3.1 Damage detection with global modal information

It can be seen from Fig. 15 that COMAC fails to identify the damages in Scenarios 1 and 2 indicating that COMAC is not a good indicator to detect the local damage of shear connectors

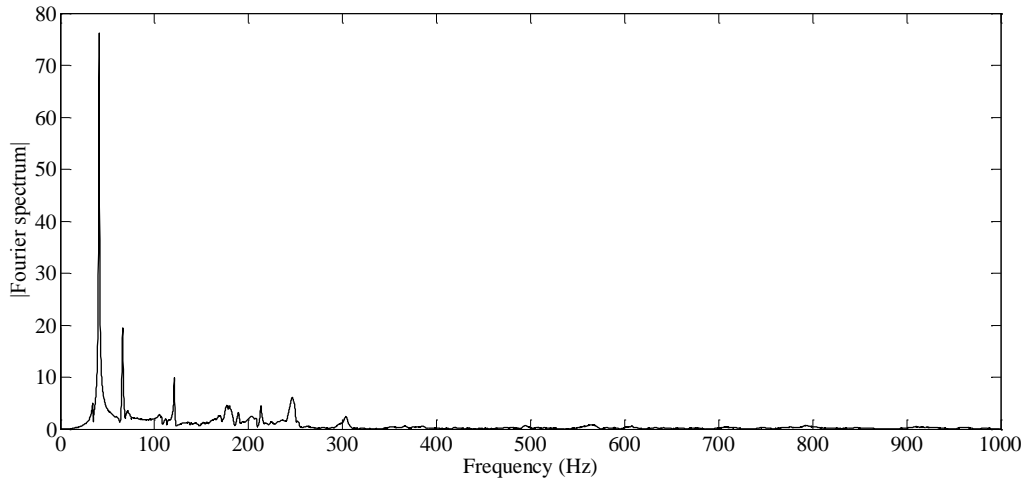


Fig. 17 Fourier spectrum of the measured response at SB5 from damage Scenario 1

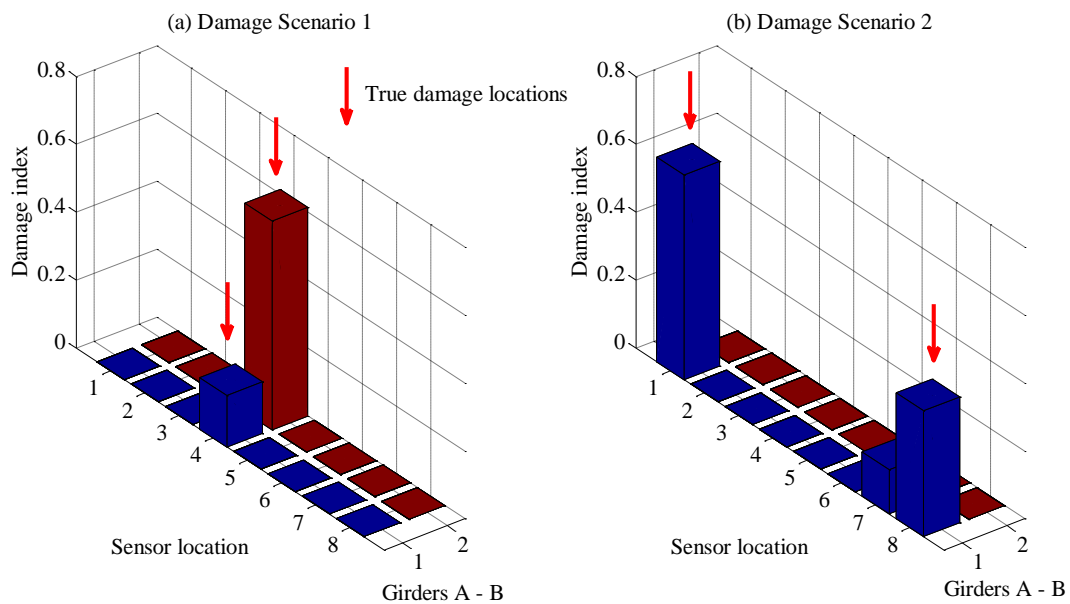


Fig. 18 Damage detection results using PSDT with data from undamaged structure available

because the identified frequency and mode shapes would be polluted by the noise effect in lab testing. Fig. 16 shows the damage detection results with changes in flexibility. It can be found that the damages in Scenario 1 are not detected correctly, while damages in Scenario 2 are identified accurately indicating that the detection using changes in flexibility is more powerful than COMAC but not applicable for the minor damage case with smaller modal information changes.

5.3.2 Damage detection with power spectral density transmissibility

The same 16384 recorded data points were used to perform the modal analysis to obtain the

FRF at each sensor location. Hanning window was used to reduce the leakage in the fast Fourier transform. PSDT vectors in the undamaged and damaged states were calculated with Eq. (14). Fig. 17 shows the Fourier spectrum of the measured response at sensor location SB5 from damage Scenario 1. As shown the magnitude of Fourier spectrum after 400 Hz is very small, therefore PSDT vectors in the frequency range of 15 Hz ~ 400 Hz are used to compute the damage index with Eq. (13) and identify the damage location of shear connectors. Since more uncertainties may exist in the experimental testing, α is set as 0.05 such that the cumulative probability of the upper confidence limit is 95%.

Figs. 18(a) and 18(b) show the identified results of Scenarios 1 and 2, respectively. It can be found from Fig. 18(a) that two damage index values at the sensor location No. 4 in two girders are obtained, indicating that the damages of shear connectors are presented in these two areas in damage Scenario 1. This observation illustrates that the introduced damage of SC7, SC8, SC23 and SC24 are identified correctly. It should be noticed that the damage index at the sensor location No. 4 in Girder B is around 0.6, while it is around 0.15 at sensor location No. 4 in Girder A although the damage severities at these two locations are the same. One possible reason for this difference is the possible different frictions between the steel girders and concrete slab. Although the two steel girders used in the structure model are the same, the surface conditions of the concrete slab at the two locations might be different owing to construction quality control, which results in different frictions between steel girders and concrete slab and hence affects the calculated damage indices at the two locations. Moreover, this observation also indicates that the absolute damage index value cannot be used to quantify the damage. This limitation is the drawback of non-model based methods, i.e., they can locate the damage but very difficult to quantify the damage. If a finite element model is involved in the analysis, the model updating and damage quantification can be conducted with the proposed PSDT concept (Li *et al.* 2015). Then the damage locations and extents in structures can be identified with the output-only vibration measurements. However, it should be noted that the reliability of the model updating approach very much depends on the accuracy of the FE model of the structure. For a civil engineering structure, it is not necessarily straightforward to establish a FE model based on design drawings to accurately represent the true structure. Model updating analysis based on inaccurate FE model may lead to inaccurate structural condition identifications. Therefore, developing condition monitoring method without the need to involve the structural model will find wide applications.

Damage detection results for Scenario 2 are shown in Fig. 18(b). It can be found that these two introduced damage locations are identified accurately. A false identification appears in sensor location No. 7 in Girder A as this area is close to the true damage location at SA8. The above results demonstrated that the proposed method with PSDT using experimental testing data to detect the damage of shear connectors gives better and more accurate results than those with global modal information, and indicates that the proposed method is more robust to the environmental and measurement noise effect.

5.4 Case B: measured data from undamaged model not available

5.4.1 Damage detection with relative difference of frequency response functions

Fig. 19 shows the damage detection results with the relative difference of FRFs between slab and girder. It can be found that the damages in both scenarios are identified, but with several false identifications, for example, sensor locations No. 3 and No. 8 of Girder B in Scenario 1, sensor location No. 5 of Girder B in Scenario 2.

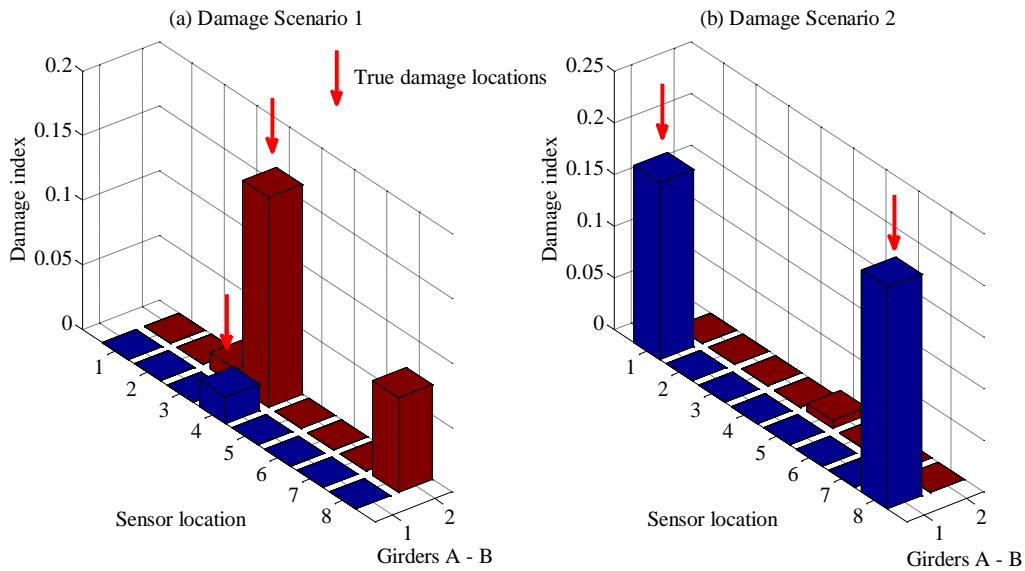


Fig. 19 Damage detection results using RDFRF without the data from the undamaged structure

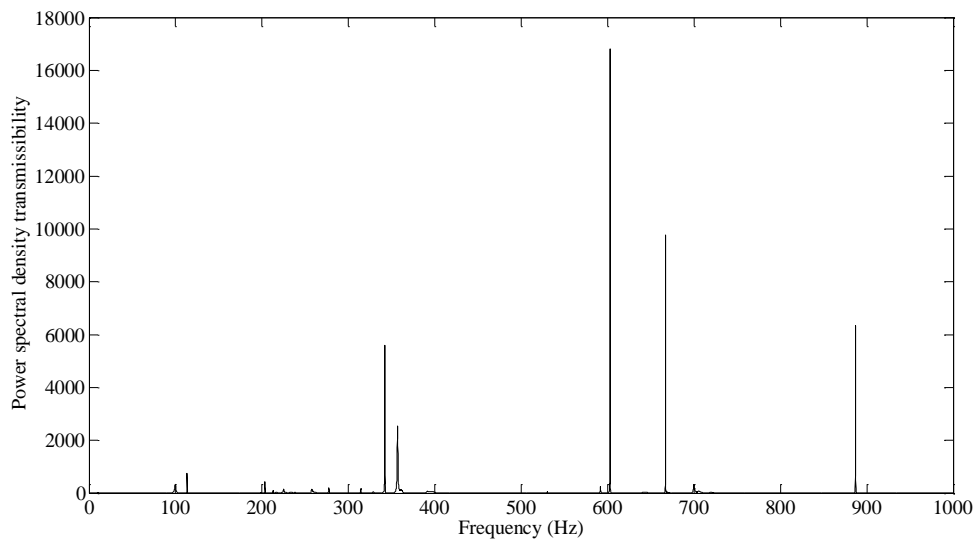


Fig. 20 Power spectral density transmissibility at sensor location SA1 of damage Scenario 1

5.4.2 Damage detection with power spectral density transmissibility

A reference sensor location is defined as shown in Fig. 13. Fig. 20 shows the PSDT from the reference sensor response to the slab response at sensor location SA1 of damage Scenario 1. It is a vector with scalar numbers covering all the frequency lines with the same order of magnitude values. Therefore, PSDT vectors in the frequency range of 15 Hz~1000 Hz are used to compute the damage index with Eq. (16). Figs. 21(a) and 21(b) show the damage detection results for Scenarios 1 and 2, respectively. It can be seen that the introduced damages of shear connectors in

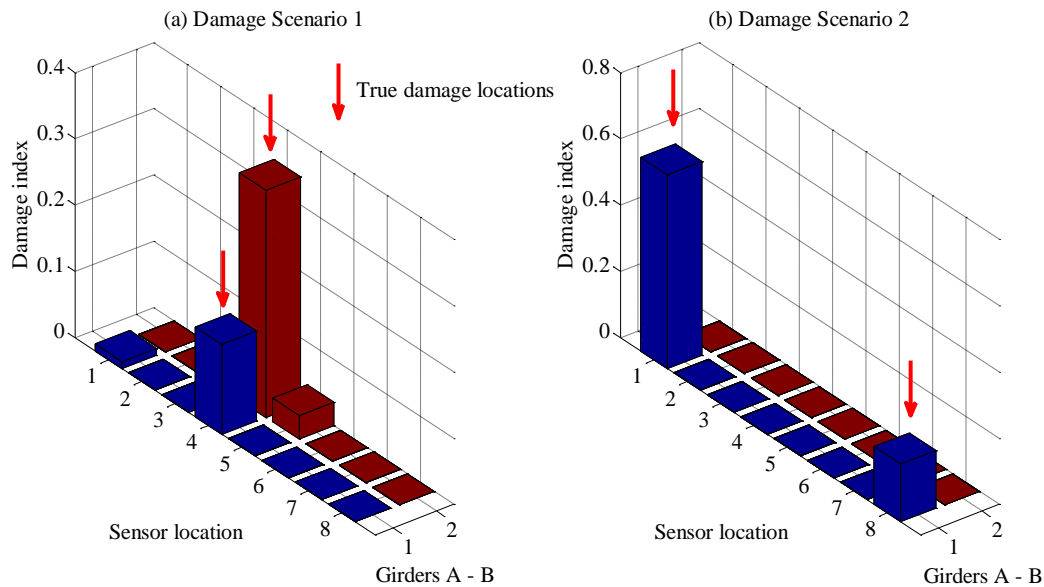


Fig. 21 Damage detection results using PSDT with data from undamaged structure unavailable

both damage scenarios are identified accurately. Several small false identifications are observed at sensor locations No. 1 in Girder A and No. 5 in Girder B of Scenario 1 and their damage index values are less than 0.05.

A comparison between Figs. 19 and 21 indicates that the proposed damage detection method with PSDT is more sensitive to the damage and can give higher damage indices and less false identifications. These results demonstrated again that the proposed condition assessment approach based on PSDT can identify the damage locations of shear connectors efficiently with and without measurement data from the undamaged structure. Although a few false identifications might occur, the proposed method can be used effectively to identify possible shear connector damages that cannot be reliably detected by routine visual inspections.

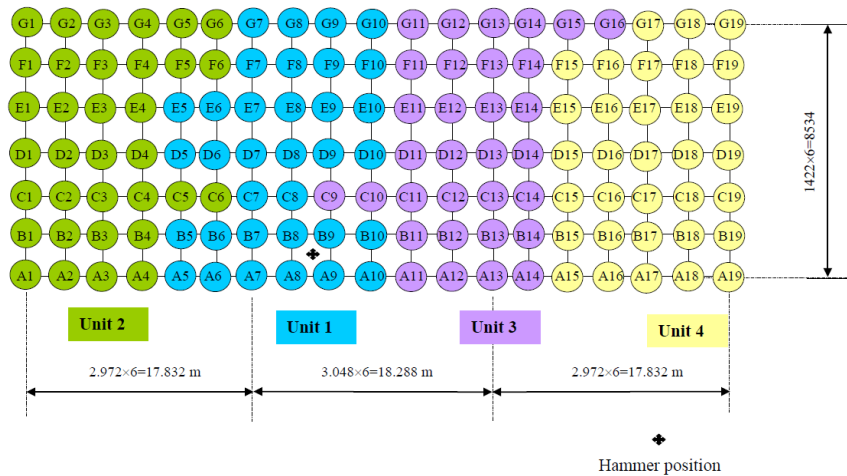
6. In-field testing

The proposed damage detection method is further applied to evaluate the shear link conditions of a real bridge. Bridge No. 852 is located on North West Coastal Highway over the Balla Balla River in the Shire of Roebourne, Western Australia. It is a pre-stressed concrete bridge constructed in 1975, which consists of three spans with an overall length of 53.95 m and width of 9.398 m. The central span of the bridge is 18.288 m and the external spans are 17.831 m. The deck of the bridge is the cast-in-situ reinforced concrete slabs supported by seven precast pre-stressed I-type girders, as shown in Fig. 22. The shear connectors are used to link the slab and girders together. They are 12 mm in diameter and enter the RC slab for a 100 mm length before being bent for anchorage. Spacing of the connectors varies from 76 mm in the ends to 381 mm in the center of the girders. More details about the design of the bridge are referred to a technical report (Xia *et al.* 2005).

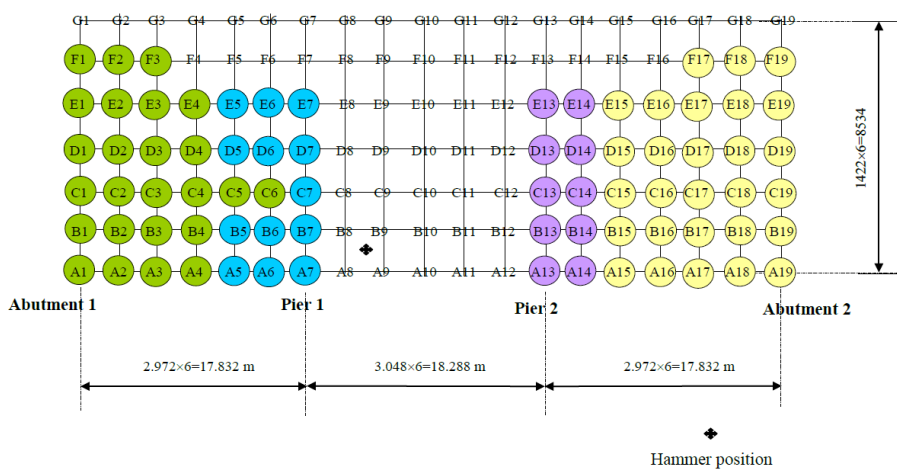
Field dynamic testing on this bridge was carried out in 2005 (Xia *et al.* 2005). The identified



Fig. 22 General view of Bridge No. 852



(a) Slab



(b) Girders

Fig. 23 Sensor placement on slab and girders

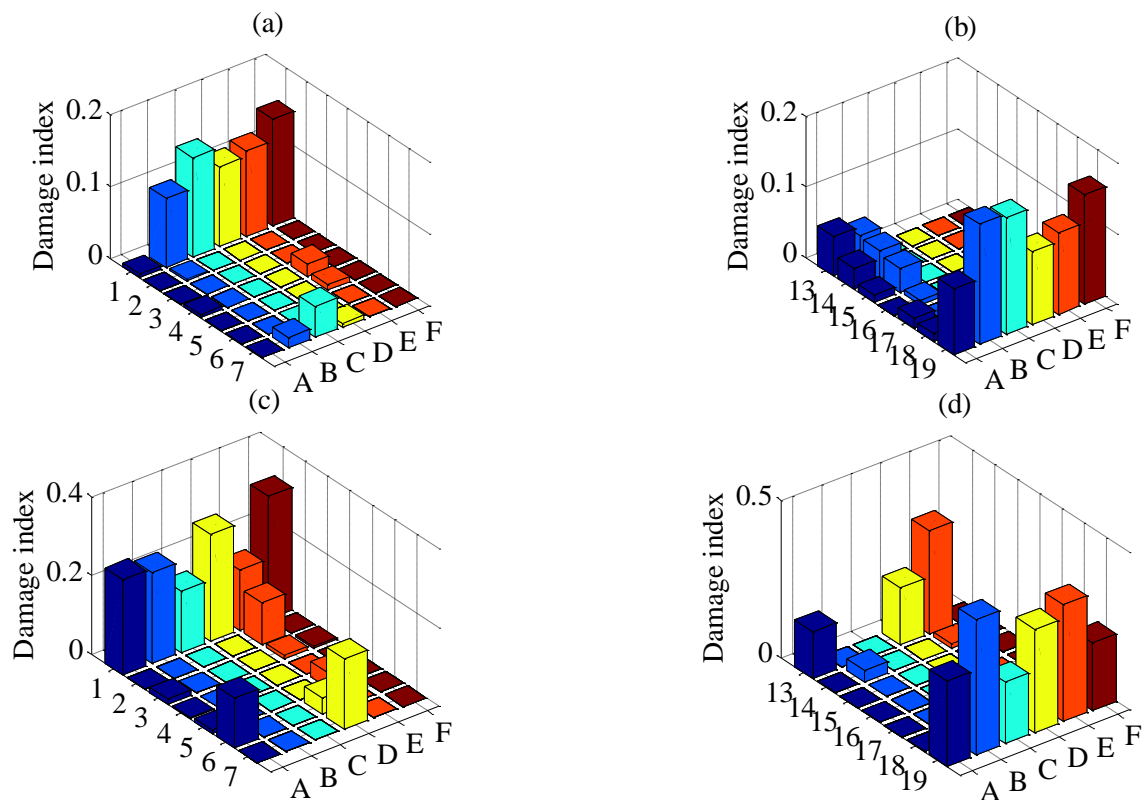


Fig. 24 Damage detection results for Bridge No. 852 (a) with RDFRF, left span; (b) with RDFRF, right span; (c) with PSDT, left span; (d) with PSDT, right span

first six natural frequencies are 6.76 Hz, 7.95 Hz, 10.06 Hz, 10.75 Hz, 11.03 Hz and 11.61 Hz, respectively. These measured acceleration data are reanalyzed in this study to identify shear link conditions. Fig. 23 shows the sensor placement on the slab and girders. The bridge has seven girders, and so accelerometers were placed on the slab locations corresponding to the seven girders, allowing comparison with the underneath girder measurements. There are nineteen sensor locations on the slab along the longitudinal direction in each row. Site condition and in-field testing safety concerns make the measurement points underneath the girders limited to the sensor locations shown in Fig. 23(b). An instrumented DYTRAN 5803A sledge hammer was used in the impact tests, and eight Kistler accelerometers were repeatedly employed to measure the acceleration responses. The sampling rate was set to 100 Hz, and 1024 data points were recorded in each impact.

FRFs were extracted from the measured acceleration response data and hammer impact force with DIAMOND toolbox. Frequency range from 1 ~ 21 Hz is used to include the first ten modes (Doebbling *et al.* 1997). Five reference sensors, e.g., A10, B10, C10, D10, E10 and F10 are defined to average the damage index. Fig. 24 shows the identification results based on the differences of FRFs and PSDT vectors. Damages of shear connectors from both methods are mostly identified at the support locations, especially near the abutments 1 and 2 as the shear forces at the supports are generally larger than those at other locations. Comparing the identification results from these two

methods, detection with PSDT gives higher damage values and indicates that it is more sensitive to the damage. The condition assessment results are reasonable since the shear connections at the support locations are more easily to be damaged. Nonetheless, this cannot be verified as the bridge is still in service. Evaluation of load carrying capacity of the bridge has been carried out by Ding *et al.* (2012).

7. Conclusions

This paper proposes a dynamic condition assessment approach based on PSDT to identify the damage of shear connectors in slab-on-girder bridge structures. The method can be used to detect shear link damages with or without measurement data of the undamaged structure. Both numerical and experimental test data demonstrate that the proposed method outperforms the traditional global modal based methods as well as the local method based on FRF differences in detecting shear link damages. The proposed method is also used to detect shear link conditions in a real bridge. Both the proposed method and FRF difference method predict the similar shear link conditions of the bridge, i.e., possible shear link damages exist near the supports of the three-span continuous bridge.

It is difficult to perform the tests with different damage severities of shear connectors in the laboratory. In practice, usually steel bars are casted into concrete slab as shear connectors. Complete failure of a shear connector is associated to the shear off of the bar or large concrete crushing failure that it no longer provides constraint on the steel bar to prevent relative movement. Partial failure comes from large excessive shear deformation of the bar or partial concrete crushing failure around the bar. If a shear link or a bolt in this study is not completely removed to create relative movement between deck and girder, large shear deformation of the bolt or concrete crushing damage around bolt needs to be introduced. Such damage could occur in a real bridge under traffic loading, but it is not likely in the lab tests under low energy level hammer excitations. This is the limitation of the conducted numerical and experimental studies.

Acknowledgments

The work described in this paper was supported by Australian Research Council Discovery Early Career Researcher Award DE140101741 “Development of a Self-powered Wireless Sensor Network from Renewable Energy for Integrated Structural Health Monitoring and Diagnosis”.

References

- Bendat, J.S. and Piersol, A.G. (1980), *Engineering Applications of Correlation and Spectral Analysis*, John Wiley & Sons, USA.
- Berczynski, S. and Wroblewski, T. (2010), “Experimental verification of natural vibration models of steel-concrete composite beams”, *J. Vib Control*, **16**(14), 2057-2081.
- Chiewanichakorn, M., Aref, A.J., Chen, S.S. and Ahn, S. (2004), “Effective flange width definition for steel-concrete composite bridge girder”, *J. Struct. Eng.*, ASCE, **130**(12), 2016-2031.
- Dilena, M. and Morassi, A. (2004), “Experimental modal analysis of steel concrete composite beams with partially damaged connection”, *J. Vib. Control*, **10**(6), 897-913.

- Dilena, M. and Morassi, A. (2009), "Vibrations of steel-concrete composite beams with partially degraded connection and applications to damage detection", *J. Sound Vib.*, **320**(1-2), 101-124.
- Ding, L., Hao, H., Xia, Y. and Deeks, A.J. (2012), "Evaluation of bridge load carrying capacity using updated finite element model and nonlinear analysis", *Adv. Struct. Eng.*, **15**(10), 1739-1750.
- Doebbling, S.W., Farrar, C.R. and Cornwell, P.J. (1997), "DIAMOND: a graphical interface toolbox for comparative modal analysis and damage identification", *Proceedings of the Sixth International Conference on Recent Advances in Structural Dynamics*, Southampton.
- Ewins, D.J. (2000), *Modal Testing: Theory, Practice and Application*, Research Studies Press Ltd., Hertfordshire, U.K.
- Gorl, E. and Link M. (2003), "Damage identification using changes of eigenfrequencies and mode shapes", *Mech. Syst. Signal Pr.*, **17**(1), 103-110.
- Johnson, T.J. and Adams, D. E. (2002), "Transmissibility as a differential indicator of structural damage", *J. Vib. Acoust.*, ASME, **124**(4), 634-641.
- Liberatore, S. and Carman, G.P. (2004), "Power spectral density analysis for damage identification and location", *J. Sound Vib.*, **274**(3-5), 761-776.
- Li, J., Hao, H. and Lo, J.V. (2015), "Structural damage identification with power spectral density transmissibility: Numerical and experimental studies", *Smart. Struct. Syst.*, **15**(1), 15-40.
- Li, J., Law, S.S. and Ding, Y. (2012), "Substructure damage identification based on response reconstruction in frequency domain and model updating", *Eng. Struct.*, **41**, 270-284.
- Li, J. and Law, S.S. (2011), "Substructural response reconstruction in wavelet domain", *J. Appl. Mech.*, ASME, **78**(4), 041010.
- Li, J. and Law, S.S. (2012), "Substructural damage detection with incomplete information of the structure", *J. Appl. Mech.*, ASME, **79**(4), 041003.
- Liu, K. and de Roeck, G. (2008), "Damage detection of shear connectors in composite bridges", *Struct. Health Monit.*, **8**(5), 345-356.
- Lieven, N.A.J. and Ewin, D.J. (1988), "Spatial correlation of mode shapes, the co-ordinate Modal Assurance Criterion (COMAC)", *Proceedings of the 6th International Modal Analysis Conference*, **1**, 690-695.
- Maia, N.M.M., Silva, J.M.M. and Almas, E.A.M. (2003), "Damage detection in structures: from mode shape to frequency response function methods", *Mech. Syst. Signal Pr.*, **17**(3), 489-498.
- Pandey, A.K., Biswas, M. and Samman, M.M. (1991), "Damage detection from changes in curvature mode shapes", *J. Sound Vib.*, **145**(2), 321-332.
- Pandey, A.K. and Biswas, M. (1994), "Damage detection in structures using changes in flexibility", *J. Sound Vib.*, **169**(1), 3-17.
- Ren, W.X., Sun, Z.S., Xia, Y., Hao, H. and Deeks, A.J. (2008), "Damage identification of shear connectors with wavelet packet energy: laboratory test study", *J. Struct. Eng.*, ASCE, **134**(5), 832-841.
- Ribeiro, A.M.R., Silva, J.M.M. and Maia, N.M.M. (2000), "On the generalisation of the transmissibility concept", *Mech. Syst. Signal Pr.*, **14**(1), 29-35.
- Ross, S.M. (2004), *Introduction to Probability and Statistics for Engineers and Scientists*, Third edition, Elsevier Academic Press, USA.
- Salawu, O.S. (1997), "Detection of structural damage through changes in frequency: a review", *Eng. Struct.*, **19**(9), 718-723.
- Worden, K. and Manson, G. (2003), "Experimental validation of a structural health monitoring methodology: part I. novelty detection on a laboratory structure", *J. Sound Vib.*, **259**(2), 323-343.
- Wroblewski, T., Jarosinska, M. and Berczynski, S. (2013), "Damage location in steel-concrete composite beams using energy transfer ratio (ETR)", *J. Theor. Appl. Mech.*, **51**(1), 91-103.
- Yan, G., Duan, Z. and Ou, J. (2010), "Damage detection for beam structures using an angle-between-string-and-horizon flexibility matrix", *Struct. Eng. Mech.*, **36**(5), 643-667.
- Yan, W.J. and Ren, W.X. (2011), "Operational modal parameter identification from power spectrum density transmissibility", *Comput. Aid. Civil Inf.*, **27**(3), 1-16.
- Yan, W.J., Ren, W.X. and Huang, T.L. (2012), "Statistic structural damage detection based on the closed-form of element modal strain energy sensitivity", *Mech. Syst. Signal Pr.*, **28**, 183-194.

- Yi, T.H., Li, H.N. and Sun, H.M. (2013), "Multi-stage structural damage diagnosis method based on "energy-damage" theory", *Smart Struct. Syst.*, **12**(3-4), 345-361.
- Yi, T.H., Li, H.N. and Gu, M. (2013). "Wavelet based multi-step filtering method for bridge health monitoring using GPS and accelerometer", *Smart Struct. Syst.*, **11**(4), 331-348.
- Xia, Y., Hao, H. and Deeks, A.J. (2007), "Dynamic assessment of shear connectors in slab-girder bridges", *Eng. Struct.*, **29**(7), 1457-1486.
- Xia, Y., Hao, H., Deeks, A.J. and Zhu, X.Q. (2008), "Condition assessment of shear connectors in slab-girder bridges via vibration measurements", *J. Bridge Eng.*, ASCE, **13**(1), 43-54.
- Xia, Y., Hao, H., Zanardo, G. and Nguyen, M. (2005), "Vibration-based damage detection of shear connectors in Nickol River bridge and Balla Balla River bridge, Part 1: preliminary study", Technical Report, ST-05-01, School of Civil and Resource Engineering, University of Western Australia.
- Xu, Z.D. and Wu, Z.S. (2007), "Energy damage detection strategy based on acceleration responses for long-span bridge structures", *Eng. Struct.*, **29**(4), 609-617.
- Zhu, X.Q., Hao, H., Uy, B., Xia, Y. and Mirza, O. (2012), "Dynamic assessment of shear connection conditions in slab-girder bridges by Kullback-Leibler distance", *Adv. Struct. Eng.*, **15**(5), 771-780.